Systems/Circuits

Two-Step Actions of Testicular Androgens in the Organization of a Male-Specific Neural Pathway from the Medial Preoptic Area to the Ventral Tegmental Area for Modulating Sexually Motivated Behavior

Masahiro Morishita,[1] Kaito Kobayashi,[1] Moeri Mitsuzuka,[1] Ryo Takagi,[1] Kota Ono,[1] Rami Momma,[1] Yousuke Tsuneoka,[2] Shuhei Horio,[3] and Shinji Tsukahara[1]

[1]Division of Life Science, Graduate School of Science and Engineering, Saitama University, Saitama 338-8570, Japan, [2]Department of Anatomy, Faculty of Medicine, Toho University, Tokyo 43-8540, Japan, and [3]Division of Endocrinology and Metabolism, National Institute for Physiological Sciences, Okazaki 444-8585, Japan

The medial preoptic area (MPOA) is a sexually dimorphic region of the brain that regulates social behaviors. The sexually dimorphic nucleus (SDN) of the MPOA has been studied to understand sexual dimorphism, although the anatomy and physiology of the SDN is not fully understood. Here, we characterized SDN neurons that contribute to sexual dimorphism and investigated the mechanisms underlying the emergence of such neurons and their roles in social behaviors. A target-specific neuroanatomical study using transgenic mice expressing Cre recombinase under the control of *Calb1*, a gene expressed abundantly in the SDN, revealed that SDN neurons are divided into two subpopulations, GABA neurons projecting to the ventral tegmental area (VTA), where they link to the dopamine system ($Calb^{VTA}$ neurons), and GABA neurons that extend axons in the MPOA or project to neighboring regions ($Calb^{nonVTA}$ neurons). $Calb^{VTA}$ neurons were abundant in males, but were scarce or absent in females. There was no difference in the number of $Calb^{nonVTA}$ neurons between sexes. Additionally, we found that emergence of $Calb^{VTA}$ neurons requires two testicular androgen actions that occur first in the postnatal period and second in the peripubertal period. Chemogenetic analyses of $Calb^{VTA}$ neurons indicated a role in modulating sexual motivation in males. Knockdown of *Calb1* in the MPOA reduced the intromission required for males to complete copulation. These findings provide strong evidence that a male-specific neural pathway from the MPOA to the VTA is organized by the two-step actions of testicular androgens for the modulation of sexually motivated behavior.

Key words: **androgen; preoptic area; sex difference; sexual behavior; sexual dimorphism; ventral tegmental area**

Significance Statement

The MPOA is a sexually dimorphic region of the brain that regulates social behaviors, although its sexual dimorphism is not fully understood. Here, we describe a population of MPOA neurons that contribute to the sexual dimorphism. These neurons only exist in masculinized brains, and they project their axons to the ventral tegmental area, where they link to the dopamine system. Emergence of such neurons requires two testicular androgen actions that occur first in the postnatal period and second in the peripubertal period. These MPOA neurons endow masculinized brains with a neural pathway from the MPOA to the ventral tegmental area and modulate sexually motivated behavior in males.

Received Feb. 27, 2023; revised Aug. 16, 2023; accepted Sep. 13, 2023.

Author contributions: M. Morishita and S.T. designed research; M. Morishita, K.K., M. Mitsuzuka, R.T., K.O., and R.M. performed research; Y.T. and S.H. contributed unpublished reagents/analytic tools; M. Morishita, K.K., M. Mitsuzuka, R.T., K.O., and R.M. analyzed data; M. Morishita and S.T. wrote the paper.

This work was supported by Grants-in-Aid for Scientific Research Grants 20K07257 (S.T.) and 21K06414 (Y.T.) and Sasakawa Scientific Research Grant 2020-4074 from the Japan Science Society (M. Morishita). We thank Jeremy Allen from Edanz (https://jp.edanz.com/ac) for editing a draft of this manuscript.

The authors declare no competing financial interests.

Correspondence should be addressed to Shinji Tsukahara at stsuka@mail.saitama-u.ac.jp.

https://doi.org/10.1523/JNEUROSCI.0361-23.2023

Introduction

Physiologic phenomena that result in a sex difference or sex specificity are controlled by brains that are themselves sexually dimorphic. Morphologic sex differences were discovered in the medial preoptic area (MPOA) of the rat brain in 1971 (Raisman and Field, 1971), and since then this area has been extensively studied to understand sexual dimorphism in the brain. Morphologic sex differences in the MPOA are also found in numerous species of fish (Yamashita et al., 2021),

amphibians (Wilczynski et al., 2003), reptiles (Krohmer and Crews, 1987), birds (Viglietti-Panzica et al., 1994), and mammals, including humans (Ayoub et al., 1983; Tobet et al., 1986; Hofman and Swaab, 1989; Roselli et al., 2004), indicating conservation of sexual dimorphism. The MPOA is studied to clarify the mechanisms that regulate social behaviors, in part because these behaviors have significant roles in reproduction (Kondo et al., 1990; Micevych and Meisel, 2017), parenting (Numan and Stolzenberg, 2009; Tsuneoka et al., 2013; Dulac et al., 2014), and aggression (Aleyasin et al., 2018). In support of the MPOA being a key region in the regulation of sex-specific social behaviors, the masculinized MPOA contains a greater number of dendritic spine synapses (Amateau and McCarthy, 2002, 2004; Wright et al., 2008; Wright and McCarthy, 2009; Lenz et al., 2013).

The MPOA in rats contains a sexually dimorphic nucleus (SDN) and is involved in sexual behavior in both sexes (Yamaguchi et al., 2018; Morishita et al., 2021). The male MPOA contains more neurons than the female MPOA (Gorski et al., 1978) and may be involved in sexual arousal (Arendash and Gorski, 1983) and sexual preference (Houtsmuller et al., 1994; Woodson et al., 2002), although its precise functions require further investigation. SDN neurons express the *Calb1* gene coding calbindin D-28K (Calb; Sickel and McCarthy, 2000), which is a calcium-binding protein that acts as a buffer, sensor, and transporter of calcium ions (Schmidt, 2012). A male-biased sex difference in Calb neurons is also present in mice (Orikasa and Sakuma, 2010), guinea pigs (Bogus-Nowakowska, 2019), musk shrews (Moe et al., 2016a), and common marmosets (Moe et al., 2016b), indicating that Calb neurons contribute significantly to establishing the sexual dimorphism of the MPOA. Sex differences in neuron numbers are considered to be established by the generation, migration, death, and/or phenotypic differentiation of neurons under the hormonal milieu in each sex (McCarthy et al., 2017; Tsukahara and Morishita, 2020). Specifically, a greater number of Calb neurons is maintained in the male SDN via testicular androgen actions during the perinatal and peripubertal periods, whereas a smaller number of Calb neurons is present in the female SDN, which does not change with ovarian estrogen actions (Orikasa and Sakuma, 2010; Gilmore et al., 2012; Morishita et al., 2017; Morishita et al., 2020). However, little is known about the physiological roles of the sexually dimorphic neural circuit assembled by Calb neurons and the mechanisms responsible for organizing the circuit.

In this study, we determined the projection site and neurotransmitter of Calb neurons in the SDN and their sex differences. We also examined the roles of androgens in organizing the sexually dimorphic Calb neuronal projection and the roles of Calb neurons in social behaviors. As a result, Calb neurons in the SDN were categorized into two subpopulations, neurons producing GABA and projecting to the ventral tegmental area (VTA; $Calb^{VTA}$ neurons) and GABA neurons that spread their axons within the MPOA or to neighboring regions ($Calb^{nonVTA}$ neurons). $Calb^{nonVTA}$ neurons were not sexually dimorphic, whereas $Calb^{VTA}$ neurons were only present in the male SDN. Next, we examined whether the formation of $Calb^{VTA}$ neurons in the male brain requires androgens during the postnatal and/or peripubertal periods. Additionally, an analysis of c-*fos* in mice displaying social behaviors was conducted, and the roles of Calb neurons in male sexual behavior were examined by chemogenetic manipulation of $Calb^{VTA}$ neurons and Calb knockdown (KD) in the MPOA.

Materials and Methods

Animals

Experimental subjects included male and female Institute of Cancer Research (ICR) mice (Sankyo Labo Service; RRID:MGI:5462094), male and female C57BL/6J mice (Sankyo Labo Service; RRID:MGI:5659121), and male mice obtained from mating male and female *Cg-Calb1*$^{tm1.1(folA/cre)Hze}$*/J mice* [Calb-dgCre B6 mice; stock #023531, The Jackson Laboratory; RRID:IMSR_JAX:023531; these mice express destabilized Cre recombinase (dgCre) controlled by the *Calb1* promoter], from crossing male Calb-dgCre B6 mice with female C57BL/6J mice or from crossing male Calb-dgCre B6 mice with female ICR mice (Calb-dgCre B6/ICR mice). dgCre stabilization is elicited by the administration of trimethoprim (TMP). We confirmed a high probability of DNA recombination by examining the brains of adult mice obtained by crossing Calb-dgCre B6 mice with Ai14 mice (stock #7914, The Jackson Laboratory; RRID:IMSR_JAX:007908) after injections of TMP (170 mg/kg body weight), which was dissolved in dimethyl sulfoxide (final concentration, 17%) and then diluted with saline, once per day for 3 consecutive days (Extended Data Fig. 1-1). This TMP dosing regimen is well established for high-efficiency TMP-inducible recombination by dgCre (Madisen et al., 2015). All animals were housed in plastic cages (225 mm deep × 340 mm wide × 155 mm high) in a room maintained at 22°C with a 12 h light/ dark cycle and free access to a standard diet and tap water. The offspring obtained from crossing transgenic mice were genotyped via PCR amplification of DNA from ear biopsies according to The Jackson Laboratory protocol. All animal procedures were approved by the Animal Care and Use Committee of Saitama University and conducted in accordance with the *Guidelines for the Care and Use of Experimental Animals* of Saitama University.

Experimental design

Neuroanatomical tracing of Calb neurons. To determine the sites to which Calb neurons project, an adeno-associated virus (AAV) vector containing *Aequorea coerulescens* green fluorescent protein (AcGFP1) and wheat germ agglutinin (WGA), which depend on Cre recombinase for expression (AAV2-CAGGS-DIO-AcGFP1-2A-tWGA-WPRE-hGHpA; 7.3×10^{11} genomic copies/ml), was injected into the left MPOA of 10- to 14-week-old Calb-dgCre B6 male and female mice ($n = 4$ for each sex). AAV2-CAGGS-DIO-AcGFP1-2A-tWGA-WPRE-hGHpA was derived from pAAV-DIO-AcGFP1-2A-tWGA-WPRE-hGHpA and was constructed by inserting an AcGFP1-2A-tWGA cassette (a gift from Yasushi Miyashita, University of Tokyo, and Yoshihiro Yoshihara, RIKEN Center for Brain Science; Ohashi et al., 2011) into pAAV-CAGGS-loxP/lox2272-MCS-loxP(R)/lox2272(R)-WPRE-hGHpA (a gift from Kazuto Kobayashi and Shigeki Kato, Fukushima Medical University). WGA serves as a trans-synaptic tracer, because WGA is transported anterogradely within axons, with some being released partly from the axon terminals into the synaptic cleft. Released WGA is then taken up by the postsynaptic neurons, thereby labeling first- and second-order neurons of a pathway (Yoshihara, 2002). The mice received intraperitoneal injections of TMP (170 mg/kg body weight) 5, 6, and 7 d after virus injection and were killed 14 d after virus injection for histologic analysis. Serial brain sections were collected at 90 µm intervals to make three intermittent section series. One section series was examined by fluorescence microscopy to determine virus-infected Calb neurons in the MPOA. The other two section series were immunostained for WGA to explore the sites of Calb neuron projection and for WGA and tyrosine hydroxylase (TH) to observe WGA- and TH-immunopositive (WGA^+/TH^+) cells and WGA-immunopositive and TH-immunonegative (WGA^+/TH^-) cells in the VTA and to examine the intensity of WGA^+ signals between TH^+ cells and TH^- cells.

To determine the location of $Calb^{VTA}$ neurons in the MPOA and any sex difference in this anatomy, a mixture of AAVretro-CAG-DIO-tdTomato-WPRE-SV40pA (9.0×10^{11} genomic copies/ml; derived from pAAV-CAG-DIO-tdTomato-WPRE-SV40pA; RRID:Addgene_28306; a gift from Edward Boyden via Addgene) and AAV2-hSyn-EGFP-WPRE-bGHpA (1.3×10^{11} genomic copies/ml; derived from pAAV-hSyn-EGFP-WPRE-bGHpA; RRID:Addgene_105539; a gift from James M.

Wilson via Addgene) was injected into the left VTA of 10- to 14-week-old Calb-dgCre B6 male ($n = 6$) and female ($n = 5$) mice. The mice were intraperitoneally injected with TMP (170 mg/kg body weight) 5, 6, and 7 d after virus injection and were then killed 14 d after virus injection for histologic analysis. Brain sections containing the VTA were immunostained for TH to evaluate the virus-infected area. Brain sections containing the MPOA were immunostained for Calb to measure the numbers of $Calb^+$ cells expressing tdTomato ($Calb^+$/$tdTomato^+$ cells; termed $Calb^{VTA}$ neurons in this study) and $Calb^+$ cells without tdTomato expression ($Calb^+$/tdTomato− cells), which we categorized as $Calb^{nonVTA}$ neurons.

GraphPad Prism software, versions 9.4 and 10.0 (RRID:SCR_002798), was used for all statistical analyses. Student's *t* test or Welch's *t* test was performed after an *F* test to assess statistical differences between WGA^+/TH^- cells and WGA^+/TH^+ cells and between sexes. Differences were considered significant at $p < 0.05$.

Determination of Calb neuron neurotransmitter. To investigate whether Calb neurons synthesize GABA, 10- to 14-week-old C57BL/6J male ($n = 5$) and female ($n = 7$) mice were subjected to surgical injection of colchicine into the lateral ventricle of the brain. The mice were killed 2 d after surgery for histologic processing. Brain sections from the mice were immunostained for Calb and vesicular GABA transporter (VGAT) and examined by fluorescence microscopy. The numbers of $Calb^+$ and/or $VGAT^+$ cells in the SDN were determined to calculate the percentage of colocalization of Calb and VGAT in $Calb^+$ cells and in $VGAT^+$ cells. Student's *t* test or Welch's *t* test was performed after an *F* test to assess statistical differences in the value between sexes.

Roles of androgens in the formation of $Calb^{VTA}$ neurons. To investigate the roles of androgens in the formation of $Calb^{VTA}$ neurons during the postnatal and/or peripubertal periods, four experimental groups were prepared for each sex (see Fig. 2*A*). Male Calb-dgCre B6 mice were subjected to neonatal castration (NC) or sham surgery on postnatal day (P)1 (the day of birth). On P20, half of the NC males were subcutaneously implanted with a silicon tube filled with cholesterol (Cho). The Cho tube was removed on P56 to end hormonal manipulation (NC/Cho males; $n = 4$). The remaining NC males were subcutaneously implanted with a silicon tube filled with testosterone (T) on P20. The T tube was removed on P56 (NC/T males; $n = 4$). The sham-operated males were castrated on P20. For half of the sham-operated males, a T tube was implanted subcutaneously on P20 and removed on P56 (Sham/T males; $n = 4$). For the other half of the sham-operated males, a Cho tube was implanted on P20 and removed on P56 (Sham/Cho males; $n = 4$).

Female Calb-dgCre B6 mice were subcutaneously injected on P1 with testosterone propionate (TP; 100 µg in 0.02 ml sesame oil) or sesame oil (0.02 ml). All females were ovariectomized on P20. For half of the oil-treated females and TP-treated females, a T tube was subcutaneously implanted on P20 and removed on P56 (Oil/T females and TP/T females, respectively; $n = 4$ for each group). For the other half of these females, a Cho tube was subcutaneously implanted on P20, and the Cho tube was removed on P56 (Oil/Cho females and TP/Cho females, respectively; $n = 4$ for each group).

The hormonally manipulated mice were subjected to an injection of a mixture of AAVretro-CAG-DIO-tdTomato-WPRE-SV40pA (9.0×10^{11} genomic copies/ml) and AAV2-hSyn-EGFP-WPRE-bGHpA (1.3×10^{11} genomic copies/ml) into the left VTA on P70, followed by TMP treatment and histologic processing as described earlier (see above, Neuroanatomical tracing of Calb neurons).

A two-way ANOVA was performed to determine the effects of neonatal and peripubertal treatments and the interactions between the main factors on the numbers of $Calb^+$/$tdTomato^+$ cells ($Calb^{VTA}$ neurons) and $Calb^+$/$tdTomato^-$ cells ($Calb^{nonVTA}$ neurons) in the left SDN. Tukey's test was used for *post hoc* analysis when the effects of the interactions between the main factors were significant.

Activity of Calb neurons during social behaviors. Sexually experienced male ICR mice (10–21 weeks old) displaying sexual behavior ($n = 7$) and aggressive behavior ($n = 6$), virgin female ICR mice (10–21 weeks old) displaying sexual behavior ($n = 7$), and primiparous female ICR mice (10–21 weeks old) displaying maternal behavior ($n = 6$) were killed 60 min after behavioral tests (see below, Behavioral analysis) for histologic processing. As controls, sexually experienced males, virgin females, and primiparous females were placed alone in their home cages for the same time as that for the behavioral tests and an additional 60 min. They were then killed ($n = 6$–7 for each test). Brain sections from these animals were immunostained for c-*fos* and Calb and then subjected to stereological analysis of c-fos^+ cells with or without Calb-immunoreactivity (c-fos^+/$Calb^+$ and c-fos^+/$Calb^-$ cells, respectively) in the left SDN. Statistical differences in the cell numbers between animals displaying social behavior and animals without the behavior were assessed by Student's *t* test or Welch's *t* test after an *F* test.

Sexual behavior in male mice with chemogenetic manipulation of $Calb^{VTA}$ neurons. A mixture of an AAVretro vector expressing a Cre recombinase-dependent mouse codon-optimized Flp recombinase (Flpo; AAVretro-EF1α-DIO-Flpo-WPRE-hGHpA, 3.0×10^{11} genomic copies/ml; derived from pAAV-EF1α-DIO-Flpo-WPRE-hGHpA; RRID:Addgene_87306; a gift from Li Zhang via Addgene; Zingg et al., 2017) and an AAV2-hSyn-EGFP-WPRE-bGHpA (1.3×10^{11} genomic copies/ml) were injected into the bilateral VTA of sexually experienced Calb-dgCre B6/ICR male mice (10–21 weeks old; see Fig. 5*A*,*B*). The males were intraperitoneally injected with TMP (170 mg/kg body weight) at 5, 6, and 7 d after virus injection. Seven days after the first virus injection, they were then injected with an AAV vector expressing hM4D(Gi)-mCherry, hM3D(Gq)-mCherry, or mCherry with Flpo activity, into the bilateral MPOA ($n = 7$–8 for each virus). The AAV vector for hM4D(Gi)-mCherry [AAV2-EF1α-fDIO-hM4D(Gi)-mCherry-WPRE-hGHpA, 6.0×10^{11} genomic copies/ml] was derived from pAAV-EF1α-fDIO-mCherry-WPRE-hGHpA (RRID:Addgene_114471; s gift from Karl Deisseroth via Addgene) and pAAV-hSyn-DIO-hM4D(Gi)-mCherry-WPRE-hGHpA (RRID:Addgene_44362; a gift from Bryan Roth via Addgene; Krashes et al., 2011). The AAV vector for hM3D(Gq)-mCherry [AAV2-EF1α-fDIO-hM3D(Gq)-mCherry-WPRE-hGHpA, 2.6×10^{11} genomic copies/ml] was derived from pAAV-EF1α-fDIO-mCherry-WPRE-hGHpA and pAAV-hSyn-DIO-hM3D(Gq)-mCherry-WPRE-hGHpA (RRID:Addgene_44361; a gift from Bryan Roth via Addgene; Krashes et al., 2011). The AAV vector for mCherry (AAV2-EF1α-fDIO-mCherry-WPRE-hGHpA, 6.0×10^{11} genomic copies/ml) was derived from pAAV-EF1α-fDIO-mCherry-WPRE-hGHpA.

The behavior of virus-injected males was evaluated by a sexual behavior test (see below, Behavioral analysis) at 1 and 2 weeks after the second virus injection. To manipulate the activity of $Calb^{VTA}$ neurons, virus-injected males were injected intraperitoneally with saline (10 µl/g body weight) or clozapine-*N*-oxide (CNO; 1 mg/kg body weight; Tocris Bioscience) containing saline 30 min before the first and second behavior tests. This manipulation was counterbalanced by injecting with saline first and CNO/saline second in half the animals and with CNO/saline first and saline second in the other half. The efficiency of chemogenetic manipulation was evaluated by a c-*fos* analysis. Males expressing mCherry or hM4D(Gi)-mCherry were killed 60 min after the second test, and males expressing hM3D(Gq)-mCherry were again injected with CNO 14 d after the second behavior test and killed 60 min after CNO injection. MPOA-containing brain sections, in which virus injection into the VTA was confirmed by observing EGFP in TH-immunostained brain sections, were immunostained for c-*fos*, and activated $Calb^{VTA}$ neurons (c-fos^+/$mCherry^+$ cells) and resting $Calb^{VTA}$ neurons (c-fos^-/$mCherry^+$ cells) were counted.

A paired *t* test was used to assess statistical differences in the evaluated behaviors between males with or without CNO treatment. The Gehan–Breslow–Wilcoxon test was used to compare the latency and incidence of behaviors between males with or without CNO treatment. A two-way repeated-measures ANOVA was performed to determine the effects of CNO treatment and laterality and the interactions between the main factors in the histologic data of males subjected to chemogenetic manipulations.

Sexual behavior of Calb KD male mice. Sexually experienced male ICR mice (10 weeks old) were injected with an AAV vector expressing EGFP and a short hairpin RNA targeting Calb mRNA (shCalb; AAV2-CMV-EGFP-U6-shCalb-hGHpA, 2.2×10^{12} genomic copies/ml; DNA sequence encoding shCalb, 5′-**GGAATTGGATATTAACAAT**TAGTGCT CCTGGTTG**ATTGTTAATATCCAATTCC**TTTTTT-3′; the nucleotides

specific to Calb are in bold) or an AAV vector expressing EGFP and a short hairpin RNA targeting luciferase mRNA (shLuc; AAV2-CMV-EGFP-U6-shLuc-hGHpA, 2.1×10^{12} genomic copies/ml; DNA sequence encoding shLuc, 5′-CCGCTGGAGAGCAACTGCATTAG TGCTCCTGGTTGATGCAGTTGCTCTCCAGCGGTTTTT-3′; the nucleotides specific to luciferase are underlined; animals injected with this vector served as controls) into the bilateral MPOA. For each virus-injected male mouse, three sexual behavioral tests (see below, Behavioral analysis) were conducted once a day on 14, 21, and 28 d after virus injection. After behavioral testing, mice were killed, and brain sections were immunostained for Calb. The virus-infected area and Calb KD efficiency were evaluated via fluorescence microscopy; five males in each group were determined to have had viral vector injected into the MPOA. A two-way repeated-measures ANOVA was performed to determine the effects of Calb KD and the number of behavioral tests and the interactions between the main factors at the end points of the behavioral tests. The Gehan–Breslow–Wilcoxon test was used to compare the latency and incidence of behaviors among groups.

General procedures

Brain surgery. For the virus injection, animals treated with mixed anesthesia (medetomidine hydrochloride, 0.24 mg/kg body weight; midazolam, 3.6 mg/kg body weight; butorphanol tartrate, 5 mg/kg body weight) were placed in a stereotaxic apparatus (SR-6M-HT, Narishige) assembled with a manipulator (SM-15 or SMM-100, Narishige), a microinjector (IMS-10 or IMS-20, Narishige), and a Neuros Syringe (7001 KH, Hamilton). The syringe needle was inserted into the MPOA (stereotaxic coordinates, 0.02 mm rostral to the bregma, 0.3 mm left or bilateral to the midline, and 5.0–5.2 mm below the dura) or VTA (stereotaxic coordinates, 3.1 mm caudal to the bregma, 0.7 mm left or bilateral to the midline, and 4.6 mm below the dura). An appropriate AAV vector solution was injected into the MPOA (volume, 0.3 µl; time, 6 min; flow rate, 0.05 µl/min) or the VTA (volume, 0.4 µl; time, 8 min; flow rate, 0.05 µl/min).

For colchicine treatment, animals anesthetized with the mixed anesthesia were placed in a stereotaxic apparatus assembled with a glass capillary filled with 2.86% colchicine in saline and connected to a syringe pump. The tip of the glass capillary was inserted into the lateral ventricle (stereotaxic coordinates, 1.0 mm caudal to the bregma, 1.0 mm left of the midline, 2.0 mm below the dura). Colchicine (100 μg in 3.5 μl saline) was then infused into the lateral ventricle at a flow rate of 0.7 μl/min for 5 min.

Hormonal manipulation. To manipulate gonadal hormone effects in the postnatal periods, male pups were castrated or subjected to sham surgery on P1 under hypothermic anesthesia, and female pups were subcutaneously injected with sesame oil (0.02 ml) with or without dissolving TP (100 µg) on P1. To manipulate testicular hormone effects in the peripubertal period, neonatally castrated male mice were implanted subcutaneously with a silicon tube (inner diameter, 1.02 mm; outer diameter, 2.16 mm; length, 10.9 mm), filled with either Cho or T (length of tube filled with substance, 6.9 mm) and sealed with silicon glue (length of glue at both tube ends, 2 mm), on P20 under isoflurane inhalation anesthesia (concentration, 1.5% in air; flow rate, 1 l/min). The implanted tube was removed on P56. Male mice that underwent sham surgery and female mice treated with vehicle or TP on P1 were gonadectomized and implanted with the silicon tube containing either Cho or T on P20. The implanted tube was removed on P56. Hormonal manipulation using the T tube can mimic the plasma T level in adult male mice (Morishita et al., 2020).

Histology

Tissue preparation. Animals killed by an intraperitoneal injection of sodium pentobarbital (60 mg/kg body weight) were transcardially perfused with 0.05 M ice-cold PBS, pH 7.4, followed by ice-cold 4% paraformaldehyde in 0.05 M phosphate buffer, pH 7.4. Brains were postfixed in the same fixative at 4°C overnight and immersed in 0.05 M phosphate buffer containing 30% sucrose at 4°C for 2–3 d. The brains were coronally sectioned at a thickness of 30 µm using a cryostat. Brain sections were collected at 90 µm intervals for examining Calb neuron projection sites, at 30 µm intervals for c-*fos* analysis, and at 60 µm intervals for other analyses.

Immunofluorescence staining and microscopy. Brain sections were treated with 5% normal goat serum (NGS) in 0.05 M PBS containing 0.1% Triton X-100 (PBST), pH 7.4, for 1 h at room temperature, reacted with primary antibodies in 5% NGS-PBST at 4°C for ~48 h, and reacted with appropriate secondary antibodies labeled with fluorescent dyes in PBST for 2 h at room temperature. Brain sections were then mounted on gelatin-coated glass slides and coverslipped using Fluoromount-G (SouthernBiotech) or DAPI Fluoromount-G (SouthernBiotech). For primary antibodies, we used a rabbit anti-WGA antibody (1:5000; catalog #T4144, Sigma-Aldrich; RRID:AB_261669), a mouse anti-TH antibody (1:4000; catalog #MAB318, Millipore; RRID:AB_2201528), a mouse anti-Calb antibody (1:5000; catalog #C9848, Sigma-Aldrich; RRID:AB_476894), a rabbit anti-VGAT antibody (1:250; catalog #AB5062P, Millipore; RRID:AB_2301998), a rabbit anti-c-*fos* antibody (1:2000; catalog #ABE457, Millipore; RRID:AB_2631318), and a rabbit anti-GFP antibody (1:10,000; catalog #ab290, Abcam; RRID:AB_303395). These antibodies have been confirmed to recognize target proteins specifically by Western blotting and/or immunocytochemistry—catalog #T4144, Sigma-Aldrich (Bráz et al., 2011); catalog #MAB318, Millipore (Shepard et al., 2006); catalog #C9848, Sigma-Aldrich (Moe et al., 2016a); catalog #AB5062P, Millipore (Wang and Sun, 2012); catalog #ABE457, Millipore (Agostinelli and Bassuk, 2021); and catalog #ab290, Abcam (Kadriu et al., 2012). As secondary antibodies we used an Alexa Fluor 568–labeled goat anti-rabbit immunoglobulin G antibody (1:800; catalog #A-11011, Thermo Fisher Scientific; RRID:AB_143157), an Alexa Fluor 647–labeled goat anti-rabbit immunoglobulin G antibody (1:800; catalog #A-21244, Molecular Probes; RRID:AB_2535812), an Alexa Fluor 647–labeled goat anti-mouse immunoglobulin G antibody (1:800; catalog #A-21235, Molecular Probes; RRID:AB_2535804), an Alexa Fluor 488–labeled goat anti-mouse immunoglobulin G antibody (1:800; catalog #A-11029, Molecular Probes; RRID:AB_2534088), and an Alexa Fluor 488–labeled goat anti-rabbit immunoglobulin G antibody (1:800; catalog A-11034, Thermo Fisher Scientific; RRID:AB_2576217).

Brain sections were observed under fluorescence microscopes BZ-9000 and BZ-X800 (Keyence), and DMI6000 B (Leica Microsystems), equipped with a complementary metal oxide semiconductor camera (ORCA-Flash4.0; Hamamatsu Photonics). To compare the intensity of WGA^+ signals between TH^+ and TH^- cells in the VTA of males injected with AAV2-CAGGS-DIO-AcGFP1-2A-tWGA-WPRE-hGHpA, the brightness of the WGA^+ signal in 35 WGA^+/TH^- cells, which were most WGA^+/TH^-cells observed in all males, and in an equal number of randomly selected WGA^+/TH^+ cells were measured using ImageJ software (National Institutes of Health; RRID:SCR_003070). To evaluate the virus-infected area, digital images of the VTA were obtained from TH-immunostained brain sections of mice injected with AAVretro-CAG-DIO-tdTomato-WPRE-SV40pA and AAV2-hSyn-EGFP-WPRE-bGHpA. The TH-immunopositive and EGFP-expressing areas in the VTA were then measured using ImageJ software. In addition, *Z*-stacked digital images of the MPOA were captured from Calb-immunostained brain sections of the mice to count the numbers of $Calb^+$/$tdTomato^+$ cells and $Calb^+$/$tdTomato^-$ cells in the SDN by visual observation. To examine colocalization of Calb and VGAT, $Calb^+$ and/or $VGAT^+$ cells in the SDN were manually counted using *Z*-stacked digital images of the MPOA in Calb-immunostained brain sections from colchicine-treated mice. To analyze the virus-infected area, TH-immunopositive and EGFP-expressing areas in the VTA were measured by ImageJ analysis of the digital images of TH-immunostained or TH- and EGFP-immunostained brain sections from mice subjected to injection of AAVretro-EF1α-DIO-Flpo-WPRE-hGHpA and AAV2-hSyn-EGFP-WPRE-bGHpA into the VTA or injection of an AAV vector expressing mCherry, hM4D(Gi)-mCherry, or hM3D(Gq)-mCherry into the MPOA. In addition, c-fos^+/$mCherry^+$ cells and c-fos^-/$mCherry^+$ cells in the SDN were counted using *Z*-stacked digital images of the MPOA in c-*fos*-immunostained brain sections.

*Stereological analysis of c-*fos *expression in Calb neurons.* Brain sections were placed in 0.6% H_2O_2-PBST for 30 min at room temperature, blocked with 5% NGS-PBST for 1 h at room temperature, reacted with a rabbit anti-c-*fos* antibody (1:2000; catalog #ABE457, Sigma-Aldrich) in 5% NGS-PBST at 4°C for ~48 h, and reacted with a goat anti-rabbit immunoglobulin conjugated to peroxidase-labeled polymer (catalog #K4003, Dako) for 30 min at room temperature. The c-*fos*-immunoreactive signal was visualized with 3,3′-diaminobenzidine (catalog #SK-4105; Vector Laboratories). c-*fos*-immunostained brain sections were placed in 0.6% H_2O_2-PBST for 30 min at room temperature, reacted with a mouse anti-Calb antibody (1:5000; catalog #C9848, Sigma-Aldrich) in PBST at 4°C for ~48 h, and reacted with goat anti-mouse immunoglobulin conjugated to peroxidase-labeled polymer (catalog #K4001, Dako) for 30 min at room temperature. Calb-immunoreactive signal was visualized using a Vector SG substrate kit (catalog #SK-4700, Vector Laboratories).

To measure the numbers of c-*fos*-expressing Calb neurons, a stereological analysis was performed using a light microscope (DM5000 B; Leica Microsystems) equipped with a charge-coupled device camera (CX9000, MBF Bioscience) and a computer running Stereo Investigator software (MBF Bioscience). The c-*fos*- and Calb-immunopositive cells (c-*fos*$^+$/Calb$^+$ cells) and c-*fos*-immunopositive and Calb-immunonegative cells (c-*fos*$^+$/Calb$^-$ cells) in the left SDN were counted using the optical fractionator method with the parameters set for stereological analysis (Extended Data Figure 3-1).

Behavioral analysis

Sexual behavior. Sexual behavior tests were conducted 2–5 h after the onset of the dark phase of the light/dark cycle in a dark room under a red dimmed light. Test animals were acclimatized to the room for >15–30 min before a test.

For c-*fos* analysis, we used sexually experienced males and estrous females, which were ovariectomized 3–5 weeks before a behavioral test, injected subcutaneously with estradiol benzoate (EB; 10 μg in 0.1 ml sesame oil) 48 h and 24 h before the test and injected subcutaneously with progesterone (P; 500 μg in 0.1 ml sesame oil) 4 h before the test. After placing an estrous female in the home cage of a sexually experienced male, the pair was observed until the male ejaculated once. We recorded the number and latency of mounts, intromissions, and ejaculations of the male and the lordosis quotient (number of lordoses/total number of mounts, intromissions, and ejaculations × 100) of the female. When males did not ejaculate within 90 min, the test was terminated, and another test was conducted 1 week later. When males ejaculated within 90 min after pairing, the pair was immediately separated, and the test animals were kept individually for 60 min and were then killed for histology.

To evaluate the effects of chemogenetic manipulation of Calb^{VTA} neurons, test males were observed for 60 min after an EB- and P-treated ovariectomized female was placed in each of their home cages. We recorded the number and latency of mounts, intromissions, and ejaculations during the test period. If the male did not act toward the female within 20 min, the paired female was replaced with another female to continue the test. The latencies of mounting and intromission were defined as the time when the first behaviors were observed after the behavior test was initiated. The latency of ejaculation was defined as the time when the first ejaculation was observed after the first intromission was observed.

For the Calb KD experiment, test males were observed for 60 min after an EB- and P-treated ovariectomized female was placed in each of their home cages. The number and latency of mounts, intromissions, and ejaculations were recorded using the same procedure as that for males in the chemogenetic manipulation experiments. We also recorded the accumulated time of sniffing and intromissions, and calculated the average duration of intromission and the intromission ratio (the number of intromissions/the numbers of mounts and intromissions).

Aggressive behavior. A resident-intruder paradigm behavioral test was conducted 2–4 h after the onset of the dark phase of the light/dark cycle in a dark room under a red dimmed light. Test male mice housed individually in their home cages were acclimatized to the room for 15 min. An intruder male mouse, in which olfaction was dysfunctional after surgical removal of the olfactory bulbs, was released in the home cage of a test male. The resident and intruder mice were then observed for 15 min to record the number, latency, and duration of aggressive behaviors. Aggressive behavior was defined as a set of behaviors including at least one of the following: chasing, boxing, wrestling, tail rattling, biting, and offensive lateral attack. If the interval between two actions did not exceed 3 s, the two actions were considered continuous and scored as one action. After the test, test animals were kept individually for 60 min and were then killed for histology.

Maternal behavior. Primiparous female mice were separated from their pups on postpartum day 3 (The day of delivery was defined as postpartum day 0.) and were subjected to a maternal behavior test on postpartum day 4, which was conducted within 4 h of the onset of the light phase of the light/dark cycle. Test animals kept in their home cages were acclimatized to an observation room for 30 min. Three pups (3–5 d old, two males and one female) were placed in three corners of the home cage that did not have a nest, and test animals were then observed for 30 min. The latency, frequency, and cumulative time of retrieving, licking, nest building, and crouching were recorded. The criteria for each behavior were as follows: Retrieving was defined as a female carrying a pup in her mouth for at least two-thirds of the distance from the corner to the nest. Licking was defined as a female licking a pup ≥3 s. Nest building was defined as a female picking up pieces of bedding. Crouching was defined as a female crouching over all three pups in the nest for more than or equal to 60 s. After removal of the pups, test animals were kept in their home cages for 60 min and were then killed for histologic analysis.

Results

Efferent projection of Calb neurons located in the MPOA

To determine the sites to which Calb neurons located in the MPOA project, an AAV vector expressing Cre recombinase-dependent AcGFP1 and WGA, a trans-synaptic anterograde tracer, (AAV2-CAGGS-DIO-AcGFP1-2A-tWGA-WPRE-hGHpA) was injected into the left MPOA of Calb-dgCre B6 mice. As a result, AcGFP1-expressing cell bodies (>100) were found in the left MPOA (Fig. 1*A*). Because of virus leaking out of the MPOA, AcGFP1-expressing cell bodies (<30) were also observed in several other brain regions, such as the anteroventral periventricular nucleus, striohypothalamic nucleus, and lateral septum (Table 1). In all animals, the left MPOA contained many AcGFP1-positive fibers and WGA$^+$ cell bodies as well as AcGFP1-positive cell bodies (Fig. 1*B*, Table 1). Additionally, many AcGFP1-positive fibers and WGA$^+$ cell bodies were found in the left VTA in all males (Fig. 1*C*, Table 1). In contrast, these markers were only observed in the left VTA of one female, but not in three other females. A small number of AcGFP1-positive fibers and WGA$^+$ cell bodies were observed in the anteroventral periventricular nucleus, striohypothalamic nucleus, accumbens nucleus, and lateral septum (Table 1). No other regions had AcGFP1-positive fibers and WGA$^+$ cells.

In the male VTA, most WGA$^+$ cell bodies showed TH immunoreactivity, but a small number of WGA$^+$ cell bodies (5–10 cells in each brain section) did not show TH immunoreactivity (Fig. 1*D–F*). AcGFP1-positive fibers were dense in the ventral part of the VTA but were sparse or absent in the dorsal part of the VTA (Fig. 1*D*). WGA$^+$/TH$^-$ cells were observed only in the ventromedial part of the VTA, whereas WGA$^+$/TH$^+$ cells were observed all over the VTA (Fig. 1*D*). WGA$^+$/TH$^+$ cells showed weaker WGA immunoreactivity, whereas WGA$^+$/TH$^-$ cells showed stronger WGA immunoreactivity. The intensity of the WGA$^+$ signal was higher in TH$^-$ cells than in TH$^+$ cells, significantly ($t_{(68)}$ = 15.16, p = 0.0005, t test; Fig. 1*G*).

Location of Calb neurons projecting from the MPOA to the VTA

To determine the location of Calb^{VTA} neurons and any sex difference, a mixture of AAVretro-CAG-DIO-tdTomato-WPRE-

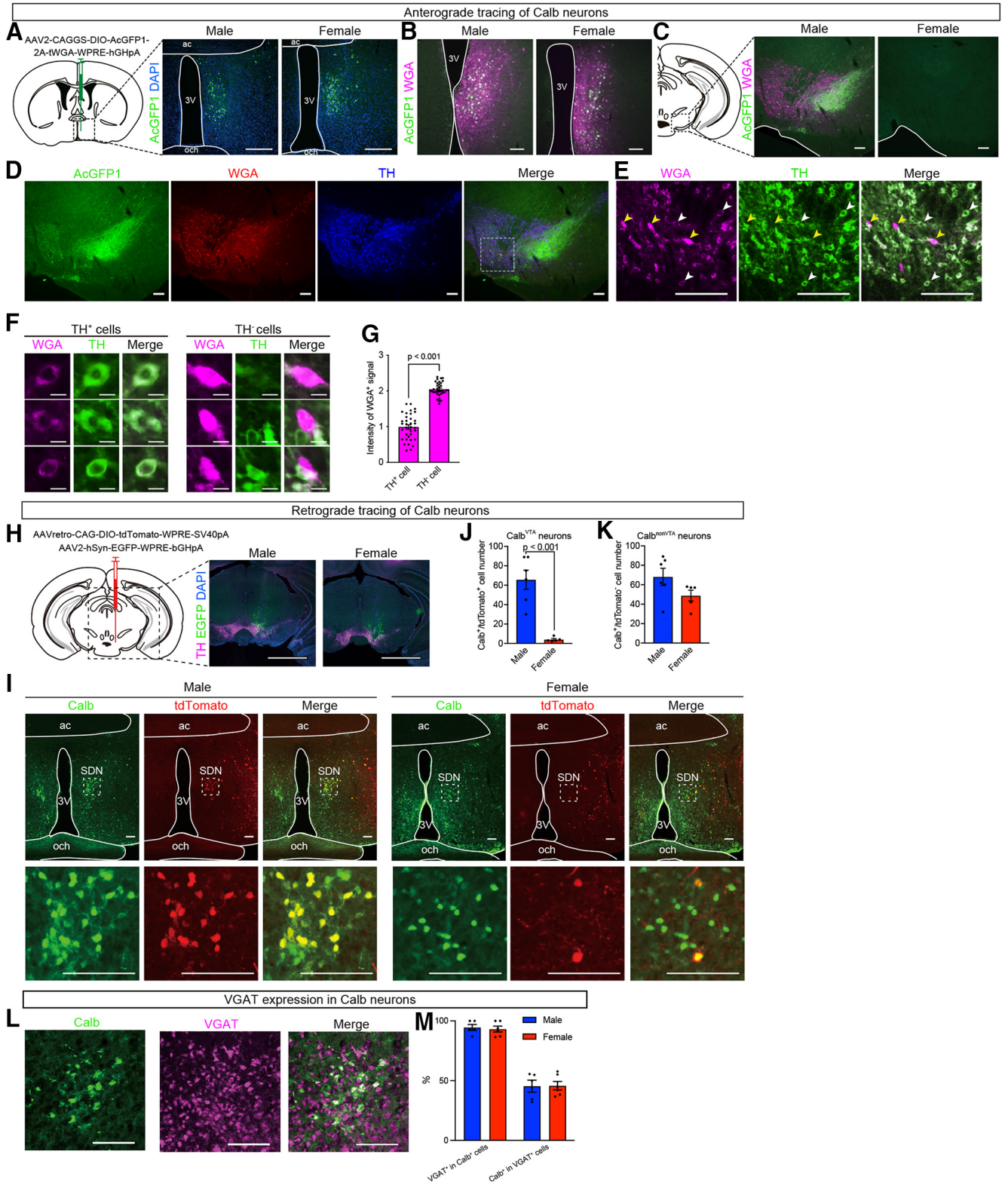

Figure 1. Male-specific projection of Calb neurons from the MPOA to the VTA. ***A***, Representative photomicrographs of the MPOA in a male and a female injected with AAV2-CAGGS-DIO-AcGFP1-2A-tWGA-WPRE-hGHpA. A high probability of TMP-inducible DNA recombination by dgCre was confirmed by examining the brains of adult mice obtained by crossing Calb-dgCre B6 mice with Ai14 mice (Extended Data Fig. 1-1). ***B***, ***C***, Representative photomicrographs of the MPOA (***B***) and VTA (***C***) in WGA-immunostained brain sections from a male and a female injected with the AAV vector. ***D***, ***E***, Representative photomicrographs of the male VTA in WGA- and TH-immunostained brain sections from a male injected with the AAV vector (***D***, ***E***). The squared region in ***D*** is shown at higher magnification in ***E***. Yellow and white arrowheads in ***E*** indicate WGA^+/TH^- and WGA^+/TH^+ cells, respectively. ***F*** shows higher magnification of the cells indicated by arrowheads in ***E***. ***G***, WGA^+ signal intensity in TH^+ and TH^- cells of the VTA. ***H***, Representative photomicrographs of the VTA in TH-immunostained brain sections from a male and a female injected with AAVretro-CAG-DIO-tdTomato-WPRE-SV40pA and AAV2-hSyn-EGFP-WPRE-bGHpA. ***I***, Representative photomicrographs of the MPOA in Calb-immunostained brain sections from a male and a female with the AAV vectors injected into the VTA. Bottom, Higher magnification of the dashed square area (top). ***J***, ***K***, The number of $Calb^+/dTomato^+$ cells ($Calb^{VTA}$ neurons, ***J***) and $Calb^+/Tomato^-$

Table 1. Distributions of AcGFP1-positive cell bodies and fibers and WGA-immunopositive cell bodies in brains injected with AAV2-CAGGS-DIO-AcGFP1-2A-tWGA-WPRE-hGHpA

		Male mice				Female mice			
Brain regions	Observation objects	#1	#2	#3	#4	#1	#2	#3	#4
Acb	AcGFP cell body	–	–	–	–	–	–	–	–
	WGA cell body and AcGFP fiber	+	–	–	–	–	–	–	–
AVPV	AcGFP cell body	–	++	–	+	+	++	–	+
	WGA cell body and AcGFP fiber	–	+	–	+	+	++	–	+
MPOA	AcGFP cell body	+++	+++	+++	+++	+++	+++	+++	+++
	WGA cell body and AcGFP fiber	+++	+++	+++	+++	+++	+++	+++	+++
LS	AcGFP cell body	++	–	–	–	–	–	–	–
	WGA cell body and AcGFP fiber	++	–	–	–	–	–	–	–
StHy	AcGFP cell body	–	–	+	–	–	–	+	–
	WGA cell body and AcGFP fiber	–	–	+	–	–	–	+	–
VTA	AcGFP cell body	–	–	–	–	–	–	–	–
	WGA cell body and AcGFP fiber	+++	+++	+++	+++	+	–	–	–

+Indicates 1–10 cell bodies and a small number of fibers; ++ indicates 11–30 cell bodies and a moderate number of fibers; +++ indicates >100 cell bodies and a large number of fibers; and – indicates no cell body and fiber was observed. Acb, accumbens nucleus; AVPV, anteroventral periventricular nucleus; LS, lateral septum; StHy, striohypothalamic nucleus.

SV40pA and AAV2-hSyn-EGFP-WPRE-bGHpA was injected into the left VTA of Calb-dgCre B6 mice. EGFP was observed in the midbrain including the VTA (Fig. 1*H*). More than 80% of the left VTA, which was determined by TH immunohistochemistry, was virus infected without a significant difference between the sexes (83.61 ± 1.55% in males and 83.17 ± 0.92% in females). The male MPOA contained many $Calb^{VTA}$ neurons, most of which were concentrated in the SDN, whereas the female MPOA contained only a few $Calb^{+}$/$tdTomato^{+}$ cells (Fig. 1*I*). Approximately half of the $Calb^{+}$ cells in the SDN expressed tdTomato in males, but a few did so in females, resulting in a significant difference in the number of $Calb^{+}$/$tdTomato^{+}$ cells ($t_{(9)} = 5.68$, $p = 0.00{,}076$, *t* test; Fig. 1*J*). However, $Calb^{+}$/$tdTomato^{-}$ cells, which can be categorized as $Calb^{nonVTA}$ neurons, were observed in the SDN of both sexes (Fig. 1*I*). The cell number did not significantly differ between the sexes (Fig. 1*K*).

Expression of VGAT in Calb neurons

VGAT immunohistochemistry was performed to examine whether Calb neurons produce GABA. Most $Calb^{+}$ cells in the SDN were $VGAT^{+}$ cells, but $VGAT^{+}$ cells in the SDN were either $Calb^{+}$ cells or $Calb^{-}$ cells (Fig. 1*L*). The percentage of colocalization of Calb and VGAT in $Calb^{+}$ cells and in $VGAT^{+}$ cells was >90% and ~50%, respectively (Fig. 1*M*). No significant difference in the values was found between the sexes.

Roles of androgens in the formation of $Calb^{VTA}$ neurons

To examine whether the emergence of $Calb^{VTA}$ neurons requires the actions of androgens during the postnatal and/or peripubertal periods, a mixture of AAVretro-CAG-DIO-tdTomato-WPRE-SV40pA and AAV2-hSyn-EGFP-WPRE-bGHpA was injected into the left VTA of Calb-dgCre B6 mice that had undergone four different hormone manipulations in each sex (Fig. 2*A*, experimental groups). Most parts of the left VTA showing TH immunoreactivity were transfected by the AAV vectors, which was confirmed by observing EGFP expression. There was no obvious difference in the location of the virus-transfected area and no significant difference in the size of this region among male groups (the percentage of virus-transfected area in the VTA, 84.39 ± 2.26% in Sham/Cho males, 81.81 ± 2.10% in Sham/T males, 83.12 ± 1.47% in NC/Cho males, and 81.69 ± 2.79% in NC/T males) or among female groups (the percentage of virus-transfected area in the VTA, 86.93 ± 10.03% in Oil/Cho females, 76.70 ± 6.36% in Oil/T females, 80.07 ± 5.38% in TP/Cho females, and 85.49 ± 2.32% in TP/T females). Nevertheless, the numbers of $Calb^{+}$/$tdTomato^{+}$ cells ($Calb^{VTA}$ neurons) and $Calb^{+}$/$tdTomato^{-}$ cells ($Calb^{nonVTA}$ neurons) observed in the SDN differed among male groups (Fig. 2*B*) and among female groups (Fig. 2*E*).

The numbers of $Calb^{VTA}$ neurons and $Calb^{nonVTA}$ neurons in the male SDN were significantly affected by NC ($F_{(1,12)} = 387.20$, $p < 0.0001$ in $Calb^{VTA}$ neurons; $F_{(1,12)} = 133.60$, $p < 0.0001$ in $Calb^{nonVTA}$ neurons; two-way ANOVA), peripubertal T treatment ($F_{(1,12)} = 301.70$, $p < 0.0001$ in $Calb^{VTA}$ neurons; $F_{(1,12)} = 7.60$, $p = 0.017$ in $Calb^{nonVTA}$ neurons; two-way ANOVA), and interaction between the main factors ($F_{(1,12)} = 317.90$, $p < 0.0001$ in $Calb^{VTA}$ neurons; $F_{(1,12)} = 6.79$, $p = 0.023$ in $Calb^{nonVTA}$ neurons; two-way ANOVA). $Calb^{VTA}$ neurons were only abundant in Sham/T males (affected by androgens in both postnatal and peripubertal periods), and the number in Sham/T males was significantly greater ($p < 0.05$) than in other males (not affected by androgens in either postnatal or peripubertal periods or in both; Fig. 2*C*). The number of $Calb^{nonVTA}$ neurons was significantly larger ($p < 0.05$) in Sham/Cho males (affected by androgens in the postnatal but not the peripubertal period) and Sham/T males than in NC/Cho males (not affected by androgens in both postnatal and peripubertal periods) and NC/T males (affected by androgens in the peripubertal period but not in the postnatal period; Fig. 2*D*). Although $Calb^{VTA}$ neuron number was greater in Sham/T males than in Sham/Cho males, the $Calb^{nonVTA}$ neuron number was significantly smaller ($p < 0.05$) in Sham/T males than in Sham/Cho males (Fig. 2*C*,*D*).

Like the SDN in Sham/T males, the SDN in TP/T females (affected by androgens in both the postnatal and peripubertal periods) contained many $Calb^{VTA}$ neurons (Fig. 2*E*). The number of $Calb^{VTA}$ neurons in the female SDN was significantly affected by neonatal TP treatment ($F_{(1,12)} = 235.20$, $p < 0.0001$; two-way ANOVA), peripubertal T treatment ($F_{(1,12)} = 317.90$, $p < 0.0001$; two-way ANOVA), and interaction between the main factors ($F_{(1,12)} = 444.60$, $p < 0.0001$; two-way ANOVA). There were significantly more $Calb^{VTA}$ neurons in TP/T females than in other groups (unaffected by androgens in either the

←

cells ($Calb^{nonVTA}$ neurons, ***K***) in the SDN. ***L***, Representative photomicrographs of the SDN in a Calb- and VGAT-immunostained brain section from a colchicine-treated male mouse. ***M***, The percentage of Calb and VGAT immunoreactivity colocalization in SDN neurons. Data indicate mean ± SEM. Black dots represent individual data points. ac, Anterior commissure; 3V, third ventricle; och, optic chiasm. Scale bars: ***A***, 300 μm; ***B–E***, ***I***, ***L***, 100 μm; ***F***, 10 μm; ***H***, and 1 mm.

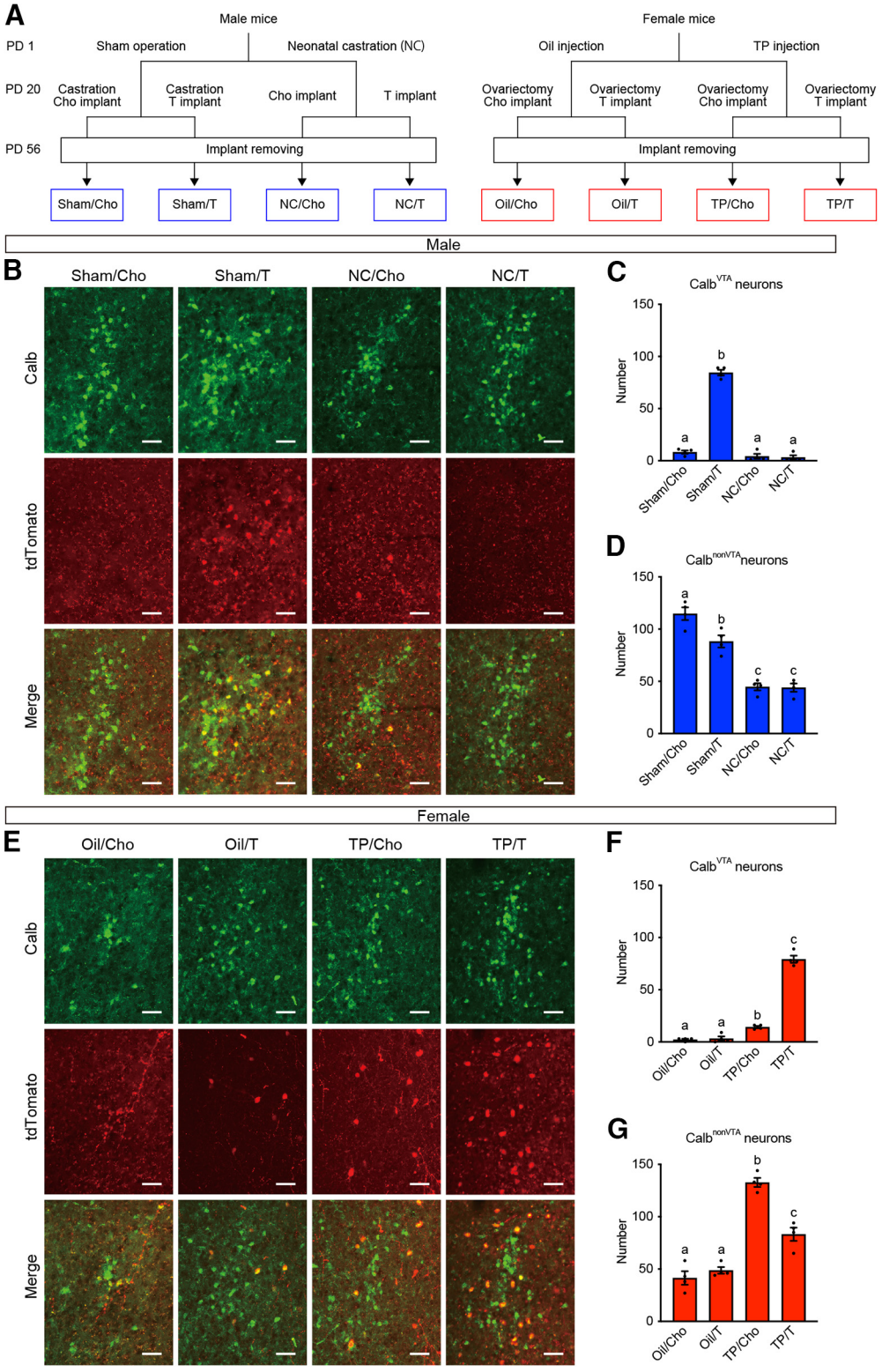

Figure 2. The roles of androgens in the emergence of Calb neurons projecting from the MPOA to the VTA. ***A***, Schematic illustration shows the hormonal manipulations of the experimental groups. ***B***, Representative photomicrographs of the SDN in Calb-immunostained brain sections from males with AAVretro-CAG-DIO-tdTomato-WPRE-SV40pA and AAV2-hSyn-EGFP-WPRE-bGHpA injected into the VTA. ***C***, ***D***, The number of $Calb^{VTA}$ neurons ($Calb^{+}$/$dTomato^{+}$ cells, ***C***) and $Calb^{nonVTA}$ neurons ($Calb^{+}$/$dTomato^{-}$ cells, ***D***) in the male SDN. ***E***, Representative photomicrographs of the SDN in Calb-immunostained brain sections from females with the AAV vectors injected into the VTA. ***F***, ***G***, The number of $Calb^{VTA}$ neurons (***F***) and $Calb^{nonVTA}$ neurons (***G***) in the female SDN. Data indicate mean ± SEM. Black dots represent individual data points. Values with different characters are significantly ($p < 0.05$) different from each other. Scale bars: 50 µm.

postnatal or peripubertal period or both; $p < 0.05$; Fig. 2*F*). $Calb^{VTA}$ neurons were also observed in the SDN in TP/Cho females (affected by androgens in the postnatal period but not in the peripubertal period), but they were significantly fewer ($p < 0.05$) than in TP/T females (Fig. 2*E*,*F*). The number of $Calb^{nonVTA}$ neurons in the female SDN was significantly affected by neonatal TP treatment ($F_{(1,12)} = 143.2$, $p < 0.0001$; two-way ANOVA), peripubertal T treatment ($F_{(1,12)} = 16.16$, $p = 0.0017$;

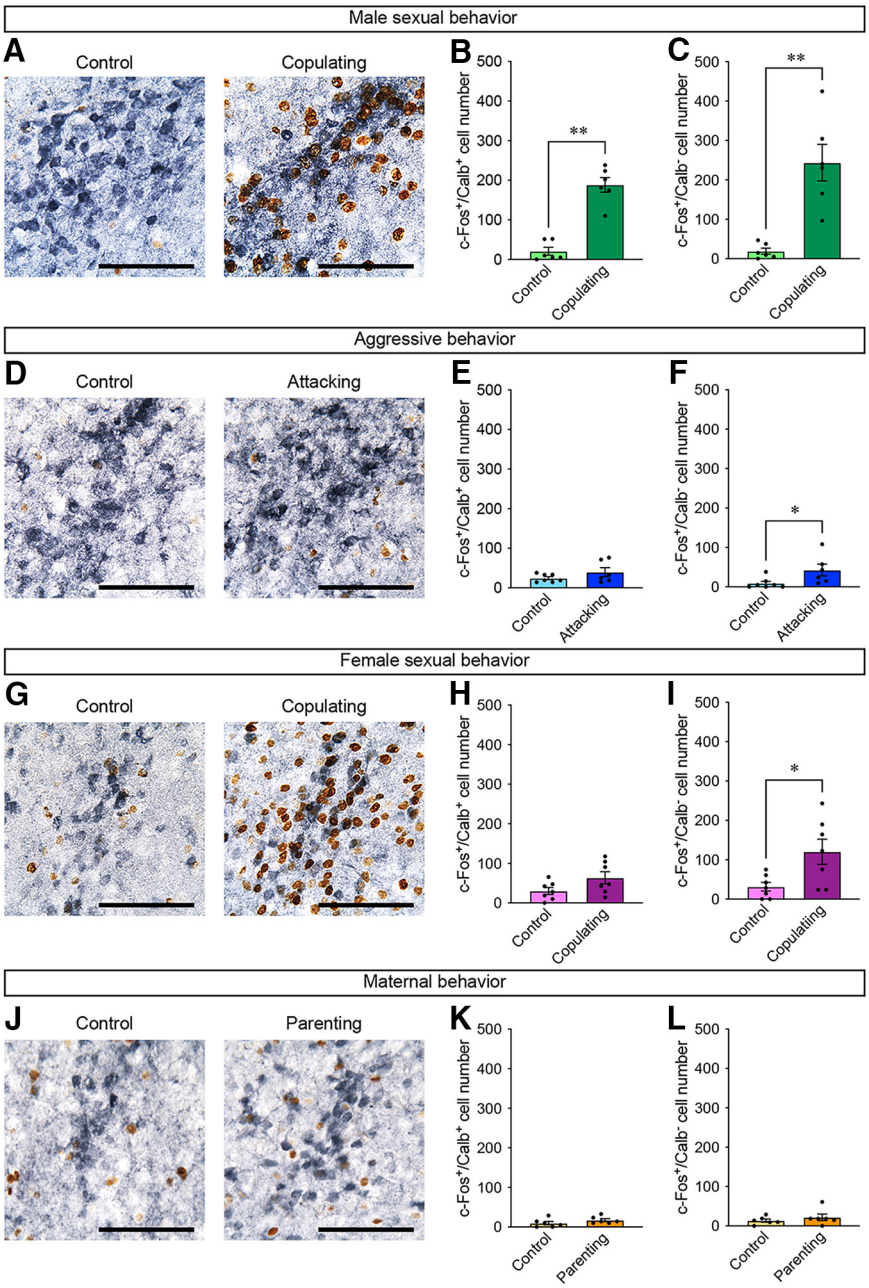

Figure 3. Calb neurons in the SDN activate during sexual behavior in male mice. ***A***, ***D***, ***G***, ***J***, Representative photomicrographs of the SDN in Calb-immunostained (blue gray) and c-*fos*-immunostained (brown) brain sections from males with or without sexual behavior (***A***) and aggressive behavior (***D***) and females with or without sexual behavior (***G***) and maternal behavior (***J***). Scale bars: 100 µm. ***B***, ***C***, ***E***, ***F***, ***H***, ***I***, ***K***, ***L***, The number of c-*fos*$^{+}$/Calb^{+} cells (***B***, ***E***, ***H***, ***K***) and c-*fos*$^{+}$/Calb^{-} cells (***C***, ***F***, ***I***, ***L***) in the SDN of males displaying sexual behavior (***B***, ***C***) and aggressive behavior (***E***, ***F***) and of females displaying sexual behavior (***H***, ***I***) and maternal behavior (***K***, ***L***). Data indicate mean ± SEM. Black dots represent individual data points; *$p < 0.05$, **$p < 0.01$. The parameters set for stereological analysis of Calb- and c-*fos*-immunostained brain sections and the performance of social behaviors in mice are shown in Extended Data Figures 3-1 and 3-2, respectively.

two-way ANOVA), and interaction between the main factors ($F_{(1,12)} = 29.16$, $p = 0.0002$; two-way ANOVA). The number of Calb$^{\text{nonVTA}}$ neurons significantly increased with neonatal TP treatment ($p < 0.05$, TP/Cho and TP/T groups vs Oil/Cho and Oil/T groups; Fig. 2*G*). Calb$^{\text{VTA}}$ neuron number was greater in TP/T females than in TP/Cho females (Fig. 2*F*). In contrast, the Calb$^{\text{nonVTA}}$ neuron number was significantly smaller in TP/T females than in TP/Cho females ($p < 0.05$; Fig. 2*G*).

Activity of Calb neurons in the SDN during social behaviors

To determine the roles of Calb neurons in the SDN during social behaviors, an immunohistochemical analysis of c-*fos* was performed using male mice that displayed sexual behavior toward female mice and aggressive behavior toward male mice and female mice that displayed sexual behavior in response to male stimuli and parenting behavior toward pups (Extended Data Fig. 3-2, behavioral profiles). Of the social behaviors observed in this study, only male sexual behavior was related to the activation of Calb neurons in the SDN (Fig. 3).

Specifically, many c-*fos*$^{+}$ cells were observed in the SDN of males that displayed sexual behavior, but only a few such cells were observed in the SDN of control males (Fig. 3*A*). There was no striking difference in the distribution and number of c-*fos*$^{+}$ cells in the SDN between the left and right sides, and therefore cells observed in the left SDN were counted. Copulating males had significantly greater numbers of c-*fos*$^{+}$/Calb^{+} cells ($t_{(10)} =$

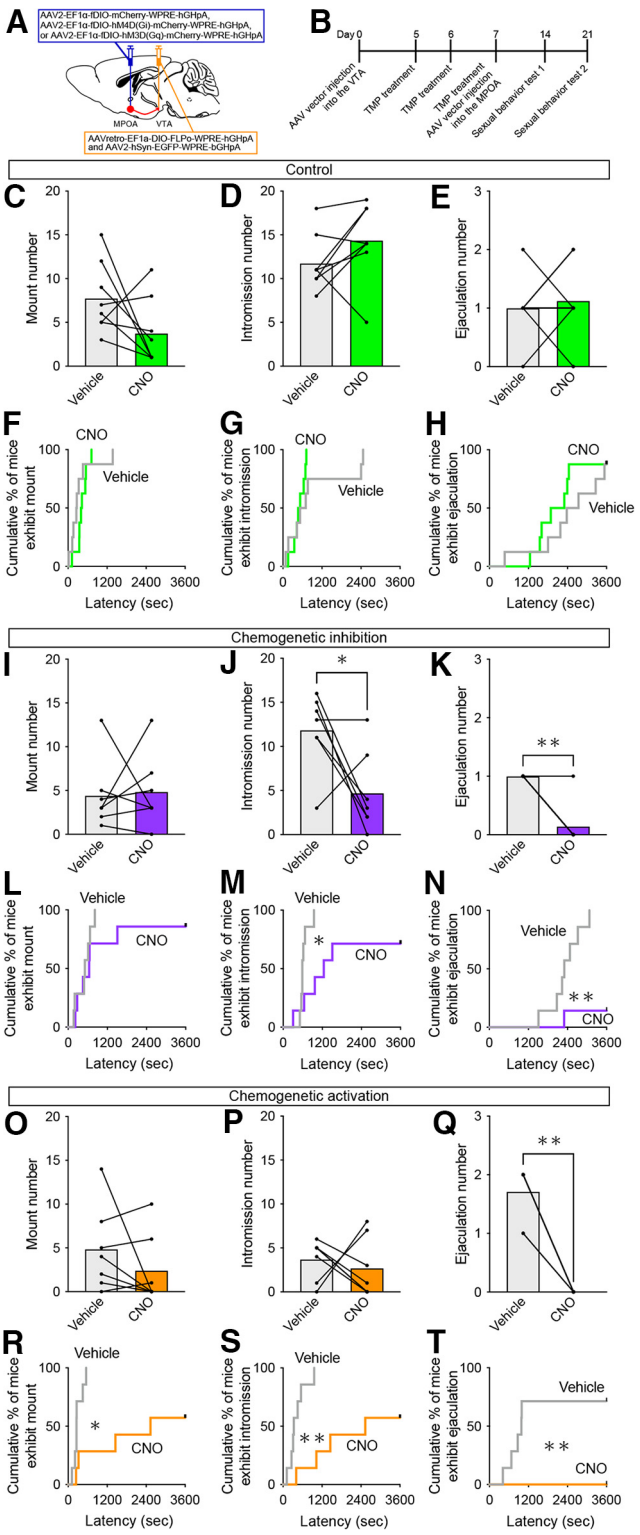

Figure 4. Chemogenetic manipulation of Calb^{VTA} neuronal cell activity changes the sexual behavior of male mice. ***A***, Schematic illustration showing AAV vector injection into the brain. ***B***, Timeline of the experiments for evaluating the effects of chemogenetic manipulation of Calb^{VTA} neurons. ***C–E***, The number of mounts, intromissions, and ejaculations in males with mCherry-expressing Calb^{VTA} neurons after treatment with vehicle or CNO (control). ***F–H***, The latency and incidence of mounts, intromissions, and ejaculations in control males after treatment with vehicle or CNO. ***I–K***, The number of mounts, intromissions, and ejaculations in males with hM4D(Gi)-mCherry-expressing Calb^{VTA} neurons after treatment with vehicle or CNO (chemogenetic inhibition). ***L–N***, The latency and incidence of mounts, intromissions, and ejaculations in the chemogenetic inhibition males after treatment with vehicle or CNO. ***O–Q***, The numbers of mounts, intromissions, and ejaculations in males with hM3D(Gq)-mCherry-expressing Calb^{VTA} neurons after treatment with vehicle or CNO (chemogenetic activation). ***R–T***, The latency and incidence of mounts, intromissions, and ejaculations in chemogenetic activation males after treatment with vehicle or CNO. Black dots represent individual data points. Black dots connected by lines indicate data from the same animals. Values of bar graphs in ***C***, ***D***, ***E***, ***I***, ***J***, ***K***, ***O***, ***P***, ***Q*** indicate the mean; *$p < 0.05$, **$p < 0.01$. The activity of Calb^{VTA} neurons after treatment with vehicle or CNO and other parameters of male sexual behavior are shown in Extended Data Figures 4-1 and 4-2, respectively.

8.01, $p < 0.0001$, t test) and c-*fos*$^+$/Calb$^-$ cells ($t_{(10)} = 8.01$, $p = 0.0008$, t test) compared with control males (Fig. 3*B*,*C*). c-*fos*$^+$ cells were observed in the SDN of males that displayed aggressive behavior toward intruder males, but they were fewer compared with those of copulating males (Fig. 3*D*). There was no significant difference in the number of c-*fos*$^+$/Calb$^+$ cells between control and attacking males (Fig. 3*E*). However, a smaller but significant number of c-*fos*$^+$/Calb$^-$ cells was found in the SDN of attacking males ($t_{(11)} = 2.28$, $p = 0.044$, t test; Fig. 3*F*). c-*fos*$^+$ cells were observed in the SDN of females that displayed sexual behavior for copulation, but most c-*fos*$^+$ cells were not Calb$^+$ cells (Fig. 3*G*). No significant difference was found in the number of c-*fos*$^+$/Calb$^+$ cells between the control and copulating females (Fig. 3*H*), although copulating females had significantly more c-*fos*$^+$/Calb$^-$ cells ($t_{(12)} = 2.64$, $p = 0.022$, t test; Fig. 3*I*). A few c-*fos*$^+$ cells were found in the SDN of females with or without parenting behavior (Fig. 3*J*). The numbers of c-*fos*$^+$/Calb$^+$ cells and c-*fos*$^+$/Calb$^-$ cells did not change with parental behavior (Fig. 3*K*,*L*).

Effects of chemogenetic manipulation of Calb^{VTA} neurons on male sexual behavior

Given the aforementioned results, we next examined the sexual behavior of Calb-dgCre male mice, in which Calb^{VTA} neurons expressed either mCherry, hM4D(Gi)-mCherry, or hM3D(Gq)-mCherry after AAV vector injection into the VTA and MPOA (Fig. 4*A*). Calb^{VTA} neuron activity was then manipulated by CNO before the behavioral performance of the mice was tested (Fig. 4*B*). The virus-transfected region in the VTA did not differ between the left and right sides or among experimental groups. EGFP expression attributed to viral transfection was observed in >80% of the VTA on the left side (82.85 ± 1.53% in the control group, 82.57 ± 1.89% in the chemogenetic inhibition group, and 84.63 ± 4.11% in the chemogenetic activation group) and on the right side (82.37 ± 2.72% in control males, 81.71 ± 4.13% in the chemogenetic inhibition group, and 93.69 ± 3.93% in the chemogenetic activation group).

CNO did not affect c-*fos* expression of Calb^{VTA} neurons in the control group (Extended Data Extended Data Fig. 4-1*A–C*), whereas CNO suppressed c-*fos* expression of Calb^{VTA} neurons in the chemogenetic inhibition group (Extended Data Fig. 4-1*D–F*). In the chemogenetic inhibition group, the number of c-*fos*-expressing Calb^{VTA} neurons was significantly decreased by CNO ($F_{(1,5)} = 375.9$, $p < 0.0001$, two-way repeated-measures ANOVA), whereas the number of Calb^{VTA} neurons without c-*fos* expression was significantly increased by CNO ($F_{(1,5)} = 14.11$, $p = 0.013$, two-way repeated-measures ANOVA). In the chemogenetic activation group, ~75% of Calb^{VTA} neurons expressed c-*fos* after CNO treatment (Extended Data Fig. 4-1*G*,*H*). The number of c-*fos*-expressing Calb^{VTA} neurons was significantly greater than the number of Calb^{VTA} neurons without c-*fos* expression in the chemogenetic activation group ($F_{(1,6)} = 27.37$, $p = 0.0020$, two-way repeated-measures ANOVA).

No significant difference was found in the parameters of the sexual behavior test between vehicle- and CNO-treated control males (Fig. 4*C–H*; Extended Data Fig. 4-2). However, although no significant effect was found in the number, latency, and incidence of mounts (Fig. 4*I*,*L*; Extended Data Fig. 4-2), chemogenetic inhibition of Calb^{VTA} neurons with CNO significantly decreased the number of intromissions ($t_{(6)} = 2.49$, $p = 0.047$, paired t test; Fig. 4*J*). In addition, chemogenetic inhibition of Calb^{VTA} neurons significantly extended and lowered the latency and incidence of intromission, respectively ($\chi^2 = 4.25$, df = 1, $p = 0.039$, Gehan–Breslow–Wilcoxon test; Fig. 4*M*). Moreover, chemogenetic inhibition of Calb^{VTA} neurons significantly decreased the number of ejaculations ($t_{(6)} = 6.00$, $p = 0.0010$, paired t test; Fig. 4*K*) and extended and lowered the latency and incidence of ejaculation, respectively ($\chi^2 = 7.86$, df = 1, $p = 0.0051$, Gehan–Breslow–Wilcoxon test; Fig. 4*N*). Chemogenetic activation of Calb^{VTA} neurons with CNO did not change the numbers of mounts and intromissions (Fig. 4*O*,*P*; Extended Data Fig. 4-2), but significantly reduced the number of ejaculations ($t_{(6)} = 9.30$, $p < 0.0001$, paired t test; Fig. 4*Q*). In addition, chemogenetic activation significantly delayed the onset and reduced the incidence of mounts ($\chi^2 = 5.44$, df = 1, $p = 0.019$, Gehan–Breslow–Wilcoxon test) and intromissions ($\chi^2 = 8.76$, df = 1, $p = 0.0031$, Gehan–Breslow–Wilcoxon test), as well as that of ejaculation ($\chi^2 = 7.00$, df = 1, $p = 0.0082$, Gehan–Breslow–Wilcoxon test; Fig. 4*R–T*).

Sexual behavior in Calb KD male mice

The effects of Calb KD on the performance of male sexual behavior were investigated by injecting AAV2-CMV-EGFP-U6-shLuc-hGHpA into the MPOA of control males and AAV2-CMV-EGFP-U6-shCalb-hGHpA into the MPOA of Calb KD males. The Calb-immunopositive signal was still observed in the virus-transfected area of the control group but was strikingly decreased in the Calb KD group (Fig. 5*A*).

Calb KD did not affect the accumulated time of male mice to sniffing estrous females (Fig. 5*B*). Calb KD males had a tendency toward a reduced number of mounts, but Calb KD did not significantly affect mount performance (Fig. 5*C–F*). However, Calb KD mice displayed significantly fewer intromissions ($F_{(1,12)} = 5.06$, $p = 0.044$, two-way repeated-measures ANOVA; Fig. 5*G*) with significant reduction of accumulated intromission time ($F_{(1,12)} = 5.54$, $p = 0.037$, two-way repeated-measures ANOVA; Fig. 5*H*). There was no significant difference in the average duration of intromission (Fig. 5*I*), intromission ratio (Fig. 5*J*), or the latency and incidence of intromission (Fig. 5*K–M*) between the control and Calb KD male mice. Calb KD had no significant effect on the number of ejaculations (Fig. 5*N*). The latency and incidence of ejaculation did not change with Calb KD in the first (Fig. 5*O*) and third tests (Fig. 5*Q*). However, in the second test, more Calb KD males showed ejaculation with shorter latency compared with the control males ($\chi^2 = 4.53$, df = 1, $p = 0.033$, Gehan–Breslow–Wilcoxon test; Fig. 5*P*). No striking difference was found in other parameters of male sexual behavior or in the lordosis quotient of the female partners (Extended Data Fig. 5-1).

Discussion

This study produced several lines of evidence to explain the sexual dimorphism of the MPOA. First, Calb neurons can be categorized into two subpopulations, GABA neurons that send axons to several regions including the MPOA but that do not project to the VTA (Calb^{nonVTA} neurons) and GABA neurons that project to and link to the dopamine system of the VTA (Calb^{VTA} neurons). Calb^{nonVTA} neurons were not sexually dimorphic. Calb^{VTA} neurons were numerous in males but scarce or absent in females, indicating that Calb^{VTA} neurons contribute significantly to sexual dimorphism. Emergence of Calb^{VTA} neurons requires testicular androgens in both the postnatal and pubertal periods. Manipulating the activity of Calb^{VTA} neurons and Calb KD in the MPOA altered the pattern of male sexual behavior. These findings indicate that Calb^{VTA} neurons endow masculinized brains with a neural pathway from the MPOA to the VTA, which plays a role in male-specific functions.

Testicular androgens in the neonatal and peripubertal periods were necessary for Calb^{VTA} neurons. Calb^{VTA} neurons did not appear without androgens in one or both periods. Calb^{VTA} neurons do not require sex chromosome genes because Calb^{VTA} neurons appeared in testosterone-treated female brains. Our data further indicate that the roles of androgens in Calb^{VTA} neurons differ between the postnatal and peripubertal periods. The total number of Calb neurons (Calb^{VTA} neurons and Calb^{nonVTA} neurons) increased when androgens were present in the postnatal period. This may be because testicular androgens during the postnatal period maintain a substantial number of SDN neurons (McCarthy et al., 2017; Tsukahara and Morishita, 2020). In the SDN without postnatal androgens, apoptotic cell death and microglia phagocytosis are promoted to reduce neuron number (Arai et al., 1996; Davis et al., 1996; Chung et al., 2000; Pickett et al., 2023). Peripubertal androgens may control the projection site of Calb neurons because peripubertal testosterone increased Calb^{VTA} neuron number and decreased Calb^{nonVTA} neuron number compared with cell numbers without peripubertal testosterone. From our data, we propose a two-step action by which testicular androgens organize a male-specific neural circuit. The first action occurs during the postnatal period to maintain a larger number of Calb neurons in the MPOA. The second action during puberty establishes the projection of Calb neurons from the MPOA to the VTA.

Establishing the MPOA–VTA projection of Calb neurons requires peripubertal androgens; however, the mechanism requires further investigation. There are several possibilities that can explain the emergence of Calb^{VTA} neurons. Peripubertal androgens (1) promote axon elongation of Calb neurons to the VTA, (2) help Calb neurons to survive after axon elongation to the VTA, and (3) induce Calb expression of non-Calb neurons that project to the VTA. In this study, peripubertal testosterone resulted in an increase in Calb^{VTA} neuron numbers and a decrease in Calb^{nonVTA} neuron number. Such a trade-off supports the notion that neurons expressing Calb until puberty become Calb^{VTA} neurons. However, Calb^{VTA} neurons arising from newly generated cells during puberty is also possible because cells born during puberty are incorporated into SDNs (Ahmed et al., 2008; Mohr and Sisk, 2013). The male SDN contained Calb^{VTA} neurons and Calb^{nonVTA} neurons in equal numbers. We previously reported that the androgen receptor (AR) is only expressed in half of the Calb neurons in the SDN of pubertal males (Morishita et al., 2020). In addition, there are twice as many Calb neurons in males in which androgens act via AR during puberty as in males without such actions or with pubertal estradiol treatment (Morishita et al., 2020). Together, it is likely that Calb neurons expressing AR during puberty are fated to be Calb^{VTA} neurons.

Dopamine neurons of the VTA play a crucial role in reward processing, motivated behaviors, and reinforcement learning (Morales and Margolis, 2017; Galaj and Ranaldi, 2021; Kim and

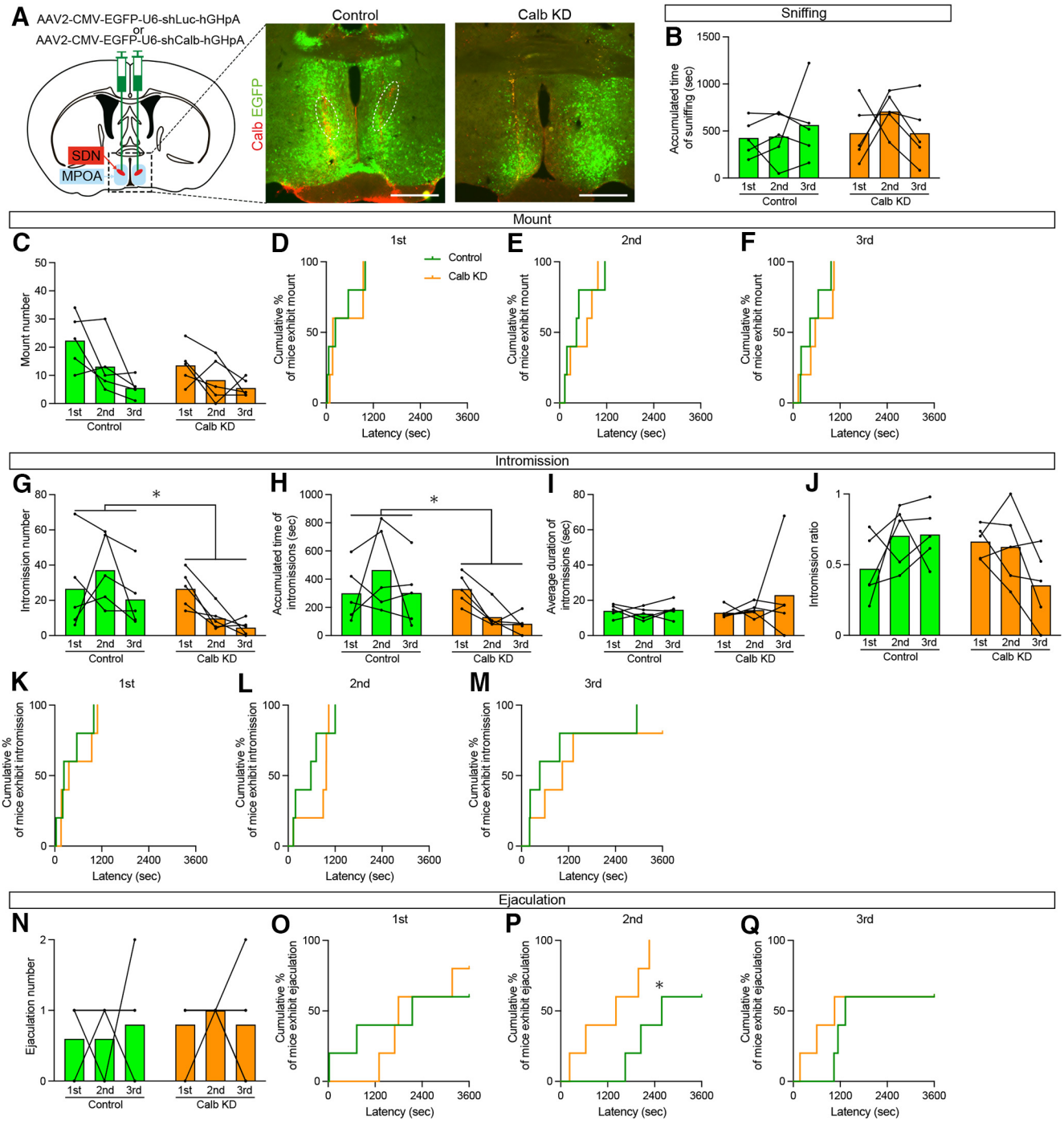

Figure 5. Sexual performance of Calb KD males. ***A***, Representative photomicrographs of Calb-immunostained brain sections from a male injected with AAV2-CMV-EGFP-U6-shLuc-hGHpA (control) and a male injected with AAV2-CMV-EGFP-U6-shCalb-hGHpA (Calb KD). The dashed regions indicate Calb-expressing cells of the SDN. Scale bars: 500 μm. ***B–F***, The accumulated time of sniffing (***B***), the number of mounts (***C***), and the latency and incidence of mounts (***D–F***) in control and Calb KD males. ***G–M***, The number of intromissions (***G***), the accumulated time of intromissions (***H***), the average duration of intromissions (***I***), the intromission ratio (***J***), and the latency and incidence of intromissions (***K–M***) in control and Calb KD males. ***N–Q***, The number of ejaculations (***N***) and the latency and incidence of ejaculations (***O–Q***) in control and Calb KD males. Values of bar graphs (***B***, ***C***, ***G***, ***H***, ***I***, ***J***, ***N***) indicate the mean of data. Black dots represent individual data points. Black dots connected by lines indicate data of the same animals; $*p < 0.05$. Other parameters of male sexual behavior and the lordosis quotient of the female partners are shown in Extended Data Figure 5-1.

Kaang, 2022). The majority of VTA neurons are dopaminergic (~65%), but the VTA also has GABA neurons (~30%) and glutamate neurons (~5%; Margolis et al., 2006; Nair-Roberts et al., 2008). These neurons integrate afferent signals with local inhibitory or excitatory inputs and generate efferent signals to control motivated behaviors (Morales and Margolis, 2017). Dopamine neurons of the VTA are tonically inhibited by GABA interneurons (Johnson and North, 1992). Optogenetic stimulation of GABA neurons in the VTA reduces the activity of neighboring dopamine neurons and of dopamine release in the nucleus accumbens, which is followed by decreased reward consummatory behavior (Morikawa and Paladini, 2011; Bourdy and Barrot, 2012; van Zessen et al., 2012). Therefore, dynamic interplay between dopamine neurons and GABA neurons within the VTA is required to

control the initiation and termination of reward consumption. In this study, TH-positive dopamine neurons were labeled with WGA originating from $Calb^{VTA}$ neurons, and the pattern of male sexual behavior, a rewarding social behavior driven by sexual motivation, was altered by manipulating $Calb^{VTA}$ neuronal activity. These findings strongly indicate that $Calb^{VTA}$ neurons link to the dopamine system in the VTA and are involved in the control of sexual motivation in male mice. However, the targets of $Calb^{VTA}$ neuronal terminals and the precise role of $Calb^{VTA}$ neurons remain undetermined.

In trans-synaptic anterograde neurotracing using WGA, the intensity of WGA-labeling becomes weaker as WGA is transported from higher-ordered neurons to lower-ordered neurons (Yoshihara, 2002). We found both WGA^+/TH^- cells and WGA^+/TH^+ cells in the VTA. The former were smaller in number but exhibited higher WGA intensity than the latter. This may indicate that many $Calb^{VTA}$ axon terminals are concentrated in nondopamine neurons, with the terminal arbores of nondopamine neurons spreading over the VTA to contact dopamine neurons. Because of the population size and innervation of dopamine neurons (Johnson and North, 1992; Margolis et al., 2006; Nair-Roberts et al., 2008), the nondopamine neurons could be GABA interneurons. Accordingly, we suggest that $Calb^{VTA}$ neurons inhibit GABA interneurons to disinhibit dopamine neurons. However, the possibility that $Calb^{VTA}$ axons terminate directly on dopamine neurons is not ruled out. Dopamine participates in sexual motivation (Giuliano and Allard, 2001) and is released in the nucleus accumbens during sexual behavior in male mice, especially during intromission and ejaculation (Sun et al., 2018, 2020). Chemogenetic inhibition of $Calb^{VTA}$ neurons delayed and reduced intromission and ejaculation. If $Calb^{VTA}$ neurons innervate GABA interneurons, this finding may indicate that $Calb^{VTA}$ neurons inhibit GABA interneurons to increase the activity of dopamine neurons during sexual behavior, resulting in higher motivation for copulation. Contrary to expectations, chemogenetic activation delayed sexual behavior and decreased the incidence of sexual behavior. However, this may not be surprising. Neurons that represent sexual satiety and reduce sexual motivation in male mice are present in the bed nucleus of the stria terminalis (Zhou et al., 2023). These neurons do not fire for a long time once activated at ejaculation. When $Calb^{VTA}$ neurons are stimulated, a large amount of dopamine may be released. Males in which $Calb^{VTA}$ neurons are chemogenetically stimulated before encountering females may fall into a sexually refractory state, and thereby sexual motivation may be lowered. This idea is supported by delayed first mount or no mount by males, which did not occur in the case of chemogentic inhibition.

Calb KD males displayed fewer intromissions and less accumulated intromission time. However, they ejaculated as the control males did. Calb KD males may achieve copulation with less intromission effort. Calb has significant roles in synaptic plasticity and learning and memory (Molinari et al., 1996; Airaksinen et al., 1997; Dumas et al., 2004; Westerink et al., 2012). Moreover, Calb attenuates field excitatory postsynaptic potentials with its Ca^{2+}-buffering action (Jouvenceau et al., 1999). The threshold to stimulate Calb neurons may decrease with Calb KD, resulting in ejaculation with fewer intromissions. The success of copulation with fewer intromissions may be better for males. However, this may not be actually the case for female partners because a high chance of pregnancy requires not only fertilization but also sufficient stimulation from intromissions (Coopersmith and Erskine, 1994).

We here described a male-specific neural pathway from the MPOA to the VTA in mice. This pathway is built by the two-step actions of testicular androgens. The first action in the postnatal period ensures that a substantial number of Calb neurons are maintained in the SDN. A significant finding of this study is that postnatal androgen action is a prerequisite for the second action during puberty. The second action allows establishment of a Calb neuronal projection to the VTA and to control sexually motivated behavior. In addition, Calb has a role in male sexual behavior. However, how perinatal and peripubertal androgens cooperate to organize masculinized brains requires further investigation. The interest and incentive for sex in humans are not present at birth but develop rapidly during puberty. They are maintained in later life but can be changed by mental illness with accompanying anhedonia (Georgiadis and Kringelbach, 2012). The male-specific neural pathway found in this study is a potential substrate underlying sexual interest and motivation. Research targeting this pathway will further the understanding of sexual dysfunction, such as hypoactive sexual desire disorder and psychogenic erectile dysfunction, and will help in the development of therapeutic approaches.

References

Agostinelli LJ, Bassuk AG (2021) Novel inhibitory brainstem neurons with selective projections to spinal lamina I reduce both pain and itch. J Comp Neurol 529:2125–2137.

Ahmed EI, Zehr JL, Schulz KM, Lorenz BH, DonCarlos LL, Sisk CL (2008) Pubertal hormones modulate the addition of new cells to sexually dimorphic brain regions. Nat Neurosci 11:995–997.

Airaksinen MS, Eilers J, Garaschuk O, Thoenen H, Konnerth A, Meyer M (1997) Ataxia and altered dendritic calcium signaling in mice carrying a targeted null mutation of the calbindin D28k gene. Proc Natl Acad Sci U S A 94:1488–1493.

Aleyasin H, Flanigan ME, Russo SJ (2018) Neurocircuitry of aggression and aggression seeking behavior: nose poking into brain circuitry controlling aggression. Curr Opin Neurobiol 49:184–191.

Amateau SK, McCarthy MM (2002) A novel mechanism of dendritic spine plasticity involving estradiol induction of prostaglandin-E2. J Neurosci 22:8586–8596.

Amateau SK, McCarthy MM (2004) Induction of PGE2 by estradiol mediates developmental masculinization of sex behavior. Nat Neurosci 7:643–650.

Arai Y, Sekine Y, Murakami S (1996) Estrogen and apoptosis in the developing sexually dimorphic preoptic area in female rats. Neurosci Res 25:403–407.

Arendash GW, Gorski RA (1983) Effects of discrete lesions of the sexually dimorphic nucleus of the preoptic area or other medial preoptic regions on the sexual behavior of male rats. Brain Res Bull 10:147–154.

Ayoub DM, Greenough WT, Juraska JM (1983) Sex differences in dendritic structure in the preoptic area of the juvenile macaque monkey brain. Science 219:197–198.

Bogus-Nowakowska K (2019) Ontogeny of neurons containing calcium-binding proteins in the preoptic area of the guinea pig: sexually dimorphic development of calbindin. Dev Neurobiol 79:175–201.

Bourdy R, Barrot M (2012) A new control center for dopaminergic systems: pulling the VTA by the tail. Trends Neurosci 35:681–690.

Bráz JM, Ackerman L, Basbaum AI (2011) Sciatic nerve transection triggers release and intercellular transfer of a genetically expressed macromolecular tracer in dorsal root ganglia. J Comp Neurol 519:2648–2657.

Chung WC, Swaab DF, De Vries GJ (2000) Apoptosis during sexual differentiation of the bed nucleus of the stria terminalis in the rat brain. J Neurobiol 43:234–243.

Coopersmith C, Erskine MS (1994) Influence of paced mating and number of intromissions on fertility in the laboratory rat. J Reprod Fertil 102:451–458.

Davis EC, Popper P, Gorski RA (1996) The role of apoptosis in sexual differentiation of the rat sexually dimorphic nucleus of the preoptic area. Brain Res 734:10–18.

Dulac C, O'Connell LA, Wu Z (2014) Neural control of maternal and paternal behaviors. Science 345:765–770.

Dumas TC, Powers EC, Tarapore PE, Sapolsky RM (2004) Overexpression of calbindin D(28k) in dentate gyrus granule cells alters mossy fiber

presynaptic function and impairs hippocampal-dependent memory. Hippocampus 14:701–709.
Galaj E, Ranaldi R (2021) Neurobiology of reward-related learning. Neurosci Biobehav Rev 124:224–234.
Georgiadis JR, Kringelbach ML (2012) The human sexual response cycle: brain imaging evidence linking sex to other pleasures. Prog Neurobiol 98:49–81.
Gilmore RF, Varnum MM, Forger NG (2012) Effects of blocking developmental cell death on sexually dimorphic calbindin cell groups in the preoptic area and bed nucleus of the stria terminalis. Biol Sex Differ 3:5.
Giuliano F, Allard J (2001) Dopamine and male sexual function. Eur Urol 40:601–608.
Gorski RA, Gordon JH, Shryne JE, Southam AM (1978) Evidence for a morphological sex difference within the medial preoptic area of the rat brain. Brain Res 148:333–346.
Hofman MA, Swaab DF (1989) The sexually dimorphic nucleus of the preoptic area in the human brain: a comparative morphometric study. J Anat 164:55–72.
Houtsmuller EJ, Brand T, de Jonge FH, Joosten RN, van de Poll NE, Slob AK (1994) SDN-POA volume, sexual behavior, and partner preference of male rats affected by perinatal treatment with ATD. Physiol Behav 56:535–541.
Johnson SW, North RA (1992) Two types of neurone in the rat ventral tegmental area and their synaptic inputs. J Physiol 450:455–468.
Jouvenceau A, Potier B, Battini R, Ferrari S, Dutar P, Billard JM (1999) Glutamatergic synaptic responses and long-term potentiation are impaired in the CA1 hippocampal area of calbindin D(28k)-deficient mice. Synapse 33:172–180.
Kadriu B, Guidotti A, Chen Y, Grayson DR (2012) DNA methyltransferases1 (DNMT1) and 3a (DNMT3a) colocalize with GAD67-positive neurons in the GAD67-GFP mouse brain. J Comp Neurol 520:1951–1964.
Kim MJ, Kaang BK (2022) Distinct cell populations of ventral tegmental area process motivated behavior. Korean J Physiol Pharmacol 26:307–312.
Kondo Y, Shinoda A, Yamanouchi K, Arai Y (1990) Role of septum and preoptic area in regulating masculine and feminine sexual behavior in male rats. Horm Behav 24:421–434.
Krashes MJ, Koda S, Ye C, Rogan SC, Adams AC, Cusher DS, Maratos-Flier E, Roth BL, Lowell BB (2011) Rapid, reversible activation of AgRP neurons drives feeding behavior in mice. J Clin Invest 121:1424–1428.
Krohmer RW, Crews D (1987) Temperature activation of courtship behavior in the male red-sided garter snake (*Thamnophis sirtalis parietalis*): role of the anterior hypothalamus-preoptic area. Behav Neurosci 101:228–236.
Lenz KM, Nugent BM, Haliyur R, McCarthy MM (2013) Microglia are essential to masculinization of brain and behavior. J Neurosci 33:2761–2772.
Madisen L, et al. (2015) Transgenic mice for intersectional targeting of neural sensors and effectors with high specificity and performance. Neuron 85:942–958.
Margolis EB, Lock H, Hjelmstad GO, Fields HL (2006) The ventral tegmental area revisited: is there an electrophysiological marker for dopaminergic neurons? J Physiol 577:907–924.
McCarthy MM, Nugent BM, Lenz KM (2017) Neuroimmunology and neuroepigenetics in the establishment of sex differences in the brain. Nat Rev Neurosci 18:471–484.
Micevych PE, Meisel RL (2017) Integrating neural circuits controlling female sexual behavior. Front Syst Neurosci 11.
Moe Y, Tanaka T, Morishita M, Ohata R, Nakahara C, Kawashima T, Maekawa F, Sakata I, Sakai T, Tsukahara S (2016a) A comparative study of sex difference in calbindin neurons among mice, musk shrews, and Japanese quails. Neurosci Lett 631:63–69.
Moe Y, Kyi-Tha-Thu C, Tanaka T, Ito H, Yahashi S, Matsuda KI, Kawata M, Katsuura G, Iwashige F, Sakata I, Akune A, Inui A, Sakai T, Ogawa S, Tsukahara S (2016b) A sexually dimorphic area of the dorsal hypothalamus in mice and common marmosets. Endocrinology 157:4817–4828.
Mohr MA, Sisk CL (2013) Pubertally born neurons and glia are functionally integrated into limbic and hypothalamic circuits of the male Syrian hamster. Proc Natl Acad Sci U S A 110:4792–4797.
Molinari S, Battini R, Ferrari S, Pozzi L, Killcross AS, Robbins TW, Jouvenceau A, Billard JM, Dutar P, Lamour Y, Baker WA, Cox H, Emson PC (1996) Deficits in memory and hippocampal long-term potentiation in mice with reduced calbindin D28K expression. Proc Natl Acad Sci U S A 93:8028–8033.
Morales M, Margolis EB (2017) Ventral tegmental area: cellular heterogeneity, connectivity and behaviour. Nat Rev Neurosci 18:73–85.
Morikawa H, Paladini CA (2011) Dynamic regulation of midbrain dopamine neuron activity: intrinsic, synaptic, and plasticity mechanisms. Neuroscience 198:95–111.
Morishita M, Maejima S, Tsukahara S (2017) Gonadal hormone-dependent sexual differentiation of a female-biased sexually dimorphic cell group in the principal nucleus of the bed nucleus of the stria terminalis in mice. Endocrinology 158:3512–3525.
Morishita M, Koiso R, Tsukahara S (2020) Actions of peripubertal gonadal steroids in the formation of sexually dimorphic brain regions in mice. Endocrinology 161:bqaa063.
Morishita M, Kamada A, Tsukahara S (2021) Neuronal activation of the sexually dimorphic nucleus of the preoptic area in female and male rats during copulation and its sex differences. Neurosci Lett 755:135915.
Nair-Roberts RG, Chatelain-Badie SD, Benson E, White-Cooper H, Bolam JP, Ungless MA (2008) Stereological estimates of dopaminergic, GABAergic and glutamatergic neurons in the ventral tegmental area, substantia nigra and retrorubral field in the rat. Neuroscience 152:1024–1031.
Numan M, Stolzenberg DS (2009) Medial preoptic area interactions with dopamine neural systems in the control of the onset and maintenance of maternal behavior in rats. Front Neuroendocrinol 30:46–64.
Ohashi Y, Tsubota T, Sato A, Koyano KW, Tamura K, Miyashita Y (2011) A bicistronic lentiviral vector-based method for differential transsynaptic tracing of neural circuits. Mol Cell Neurosci 46:136–147.
Orikasa C, Sakuma Y (2010) Estrogen configures sexual dimorphism in the preoptic area of C57BL/6J and ddN strains of mice. J Comp Neurol 518:3618–3629.
Pickett LA, VanRyzin JW, Marquardt AE, McCarthy MM (2023) Microglia phagocytosis mediates the volume and function of the rat sexually dimorphic nucleus of the preoptic area. Proc Natl Acad Sci U S A 120: e2212646120.
Raisman G, Field PM (1971) Sexual dimorphism in the preoptic area of the rat. Science 173:731–733.
Roselli CE, Larkin K, Resko JA, Stellflug JN, Stormshak F (2004) The volume of a sexually dimorphic nucleus in the ovine medial preoptic area/anterior hypothalamus varies with sexual partner preference. Endocrinology 145:478–483.
Schmidt H (2012) Three functional facets of calbindin D-28k. Front Mol Neurosci 5:25.
Shepard JD, Chuang DT, Shaham Y, Morales M (2006) Effect of methamphetamine self-administration on tyrosine hydroxylase and dopamine transporter levels in mesolimbic and nigrostriatal dopamine pathways of the rat. Psychopharmacology (Berl) 185:505–513.
Sickel MJ, McCarthy MM (2000) Calbindin-D28k immunoreactivity is a marker for a subdivision of the sexually dimorphic nucleus of the preoptic area of the rat: developmental profile and gonadal steroid modulation. J Neuroendocrinol 12:397–402.
Sun F, et al. (2018) A Genetically encoded fluorescent sensor enables rapid and specific detection of dopamine in flies, fish, and mice. Cell 174:481–496.e19.
Sun F, Zhou J, Dai B, Qian T, Zeng J, Li X, Zhuo Y, Zhang Y, Wang Y, Qian C, Tan K, Feng J, Dong H, Lin D, Cui G, Li Y (2020) Next-generation GRAB sensors for monitoring dopaminergic activity *in vivo*. Nat Methods 17:1156–1166.
Tobet SA, Zahniser DJ, Baum MJ (1986) Sexual dimorphism in the preoptic/anterior hypothalamic area of ferrets: effects of adult exposure to sex steroids. Brain Res 364:249–257.
Tsukahara S, Morishita M (2020) Sexually dimorphic formation of the preoptic area and the bed nucleus of the stria terminalis by neuroestrogens. Front Neurosci 14:797.
Tsuneoka Y, Maruyama T, Yoshida S, Nishimori K, Kato T, Numan M, Kuroda KO (2013) Functional, anatomical, and neurochemical differentiation of medial preoptic area subregions in relation to maternal behavior in the mouse. J Comp Neurol 521:1633–1663.
van Zessen R, Phillips JL, Budygin EA, Stuber GD (2012) Activation of VTA GABA neurons disrupts reward consumption. Neuron 73:1184–1194.
Viglietti-Panzica C, Aste N, Balthazart J, Panzica GC (1994) Vasotocinergic innervation of sexually dimorphic medial preoptic nucleus of the male Japanese quail: influence of testosterone. Brain Res 657:171–184.

Wang X, Sun QQ (2012) Characterization of axo-axonic synapses in the piriform cortex of *Mus musculus*. J Comp Neurol 520:832–847.
Westerink RH, Beekwilder JP, Wadman WJ (2012) Differential alterations of synaptic plasticity in dentate gyrus and CA1 hippocampal area of Calbindin-D28K knockout mice. Brain Res 1450:1–10.
Wilczynski W, Yang EJ, Simmons D (2003) Sex differences and hormone influences on tyrosine hydroxylase immunoreactive cells in the leopard frog. J Neurobiol 56:54–65.
Woodson JC, Balleine BW, Gorski RA (2002) Sexual experience interacts with steroid exposure to shape the partner preferences of rats. Horm Behav 42:148–157.
Wright CL, McCarthy MM (2009) Prostaglandin E2-induced masculinization of brain and behavior requires protein kinase A, AMPA/kainate, and metabotropic glutamate receptor signaling. J Neurosci 29:13274–13282.
Wright CL, Burks SR, McCarthy MM (2008) Identification of prostaglandin E2 receptors mediating perinatal masculinization of adult sex behavior and neuroanatomical correlates. Dev Neurobiol 68:1406–1419.
Yamaguchi S, Abe Y, Maejima S, Tsukahara S (2018) Sexual experience reduces neuronal activity in the central part of the medial preoptic nucleus in male rats during sexual behavior. Neurosci Lett 685:155–159.
Yamashita J, Nishiike Y, Fleming T, Kayo D, Okubo K (2021) Estrogen mediates sex differences in preoptic neuropeptide and pituitary hormone production in medaka. Commun Biol 4:948.
Yoshihara Y (2002) Visualizing selective neural pathways with WGA transgene: combination of neuroanatomy with gene technology. Neurosci Res 44:133–140.
Zhou X, Li A, Mi X, Li Y, Ding Z, An M, Chen Y, Li W, Tao X, Chen X, Li Y (2023) Hyperexcited limbic neurons represent sexual satiety and reduce mating motivation. Science 379:820–825.
Zingg B, Chou XL, Zhang ZG, Mesik L, Liang F, Tao HW, Zhang LI (2017) AAV-mediated anterograde transsynaptic tagging: mapping corticocollicular input-defined neural pathways for defense behaviors. Neuron 93:33–47.